Atmospheric Research 272 (2022) 106153

Contents lists available at ScienceDirect

Atmospheric Research

journal homepage: www.elsevier.com/locate/atmosres

Wind stilling ceased in the Iberian Peninsula since the 2000s

Eduardo Utrabo-Carazo [a,b,*], Cesar Azorin-Molina [a], Encarna Serrano [b], Enric Aguilar [c], Manola Brunet [c], Jose A. Guijarro [d]

[a] Spanish National Research Council (CSIC), Centro de Investigaciones sobre Desertificación CIDE (CSIC-UV-GVA), Spain
[b] Departamento de Física de la Tierra y Astrofísica, Facultad CC. Físicas, Universidad Complutense de Madrid, Spain
[c] Universitat Rovira i Virgili, Centre for Climate Change, Tarragona, Spain
[d] State Meteorological Agency (AEMET), Delegation of the Balearic Islands, Palma de Mallorca, Spain

ARTICLE INFO

Keywords:
Surface Wind speed
Wind gusts
Iberian Peninsula
Atmospheric circulation
Stilling
Reversal

ABSTRACT

This study analyses quality controlled and homogenized near-surface wind speed series (SWS) at 87 meteorological stations distributed across Spain and Portugal for 1961–2019. Multidecadal variability analysis of both mean and gusts SWS confirms for the first time in the region the cessation of the *stilling* (decline of SWS) and a possible weak *reversal* phenomenon (increase in SWS) in the last decades, varying its onset from 1999 to 2018, depending on the season and variable. Different atmospheric circulation drivers are evaluated to explain the *stilling* and *reversal* phenomena. Among the chosen teleconnection indices, the Western Mediterranean Oscillation index (WeMOi) is the one that presents the highest (positive) correlation with SWS, although the correlation (negative) with the North Atlantic Oscillation index and the Mediterranean Oscillation index in winter is also statistically significant ($p < 0.05$). Results show that the interannual variability of the WeMOi could exert a strong influence on both the *stilling* and *reversal* phenomena, as it displays statistically significant negative trends for 1961–2010 and positive ones (non-significant) for 2010–2019, in agreement with the observed SWS trends. The use of the Jenkinson and Collison weather type classification reveals the marked influence of certain weather types in modulating SWS changes (*i.e.*, west, northwest, and anticyclonic types). We proposed the increase in atmospheric thermal stability and the northward shift of the jet stream as principal causes of the *stilling* phenomenon in this region. Our results improve our understanding of wind changes, and highlight the importance of regional assessments to discern their socioeconomic and environmental impacts.

1. Introduction

The effects of climate change on variables such as air temperature or precipitation have been extensively studied in recent decades (IPCC, 2013). However, less attention has been paid to near-surface wind speed (SWS) despite its socioeconomic and environmental impacts on a wide array of spheres, such as wind power industry (Tian et al., 2019; Zeng et al., 2019), evapotranspiration processes (McVicar et al., 2012a, 2012b), marine food chains (Kahru et al., 2010), air quality (Wu et al., 2018) and wind-related disasters (He et al., 2021), among many others.

Until the last two decades, scientists were sceptical about SWS changes due to several issues (Azorin-Molina et al., 2014), mainly related to the low quality and inhomogeneities of wind data derived from *e.g.*, changes in anemometer type, anemometer height or station relocations, which makes the analysis of trends and variability a challenging task (Pryor et al., 2009; Wan et al., 2010). Furthermore, there is great uncertainty in the response of atmospheric circulation to a warming climate from both a theoretical and observational point of view (Shepherd, 2014). As the SWS is mainly controlled by internal decadal ocean-atmosphere oscillations (Zeng et al., 2019), the attribution of its climate variability and changes is complex; this also explains the inability of the state-of-the-art models to accurately simulate SWS, since internal variability introduces uncertainties into the simulations performed by these models (Sun et al., 2018; Deser, 2020). This is verified through the inconsistencies between the observational data and those obtained by atmospheric reanalysis and climate simulations (Torralba et al., 2017; Deng et al., 2021; Molina et al., 2021), particularly in areas of complex topography (Ramon et al., 2019; Wohland et al., 2019).

Observational data analysis revealed a general decline in SWS in continental regions of the mid- and tropical-latitudes for 1978–2010 (Zeng et al., 2019), such as: Australia (McVicar et al., 2008), contiguous US (Pryor et al., 2009), Canada (Wan et al., 2010), China (Guo et al.,

* Corresponding author at: Centro de Investigaciones sobre Desertificación (CIDE), Ctra. CV-315 km 10,5, 46113 Moncada, Valencia, Spain.
E-mail address: eduardo.utrabo@ext.uv.es (E. Utrabo-Carazo).

https://doi.org/10.1016/j.atmosres.2022.106153
Received 19 December 2021; Received in revised form 24 February 2022; Accepted 21 March 2022
Available online 26 March 2022

2011; Zhang et al., 2020), Korea (Kim and Paik, 2015), Spain and Portugal (Azorin-Molina et al., 2014; Lorente-Plazas et al., 2015; Azorin-Molina et al., 2016), Sweden (Minola et al., 2016) and Saudi Arabia (Azorin-Molina et al., 2018b); being this decline more pronounced for stronger winds (Vautard et al., 2010) and at higher elevations (McVicar et al., 2010). This was termed as the *stilling* phenomenon by Roderick et al. (2007) and quantified in $-0.140\,m\,s^{-1}\,dec^{-1}$ (McVicar et al., 2012a). On the contrary, SWS has increased at high latitudes (*i.e.*, >65°; McVicar et al., 2012a) and on ocean surfaces (Young and Ribal, 2019) during that same period. McVicar et al. (2012a) and Wu et al. (2018) conducted a comprehensive global review in this matter.

Plausible hypothesis discussed in the literature for the *stilling* phenomenon include:

- Increased surface roughness (Vautard et al., 2010; Wever, 2012; Zhang et al., 2019), either through vegetation growth (Zeng et al., 2018), land use changes (Li et al., 2019) or urbanization (Hou et al., 2013).
- Decadal ocean-atmosphere oscillations, caused by the internal variability of the climate system (*e.g.*, Zeng et al., 2019).
- Instrumental artifacts related to the loss of cup anemometer performance because of *e.g.*, wear and tear with the mass addition of dirt to the cups and the internal bearings; rotor damage due to severe storms; and failure at the opto-electronic output signal system (Azorin-Molina et al., 2018a).

According to recent studies, the interruption of the *stilling* with a recovery of SWS, a phenomenon known as *reversal*, has occurred since the ~2010s at the regional scale *e.g.*: Sweeden (Minola et al., 2021b), China (Li et al., 2018; Zha et al., 2019; Zhang and Wang, 2020; Ge et al., 2021), Korea (Kim and Paik, 2015) and Saudi Arabia (Azorin-Molina et al., 2018b), and at the global scale, with an average increase in wind speed of $+0.240\,m\,s^{-1}\,dec^{-1}$ (Zeng et al., 2019). All these recent investigations pointed out that internal decadal ocean-atmosphere oscillations are the dominant drivers of SWS changes compared to Earth's greening (Zeng et al., 2018). However, it is not possible to rule out that the rest of the causes mentioned above have a non-negligible contribution to both the *stilling* and the *reversal* phenomena (Minola et al., 2021b), or that their importance could even vary regionally.

Since current *in-situ* wind observations are not particularly long (mainly since the ~1960s onwards), the study of internal climate variability of winds becomes especially challenging. Therein lies the novelty of this work, as it compiles, homogenizes, and analyses the largest wind speed and gust dataset available for the Iberian Peninsula (IP), combining climate records from Spain and Portugal.

The overall goal of this research is to revisit previous studies in the IP on monthly mean wind speed (Azorin-Molina et al., 2014) and daily peak wind gusts (Azorin-Molina et al., 2016), updating them to the 59-yr 1961–2019 period. According to the state-of-the-art, this is one of the longest assessment of trends and multi-decadal variability in observed SWS (McVicar et al., 2012a; Wu et al., 2018), also evaluating changes in both mean and extreme winds at the same time.

More specifically, particular objectives of this study are:

1. To determine for the first time the cease of the *stilling* and the beginning of the *reversal* in the IP over the last decade(s), identifying its onset year and its magnitude.
2. To deepen into the relation between atmospheric circulation changes and observed SWS trends in a mid-latitude region.

Section 2 covers a description of the data and analysis methods used; Section 3 presents the results; Section 4 discusses the principal findings against the state-of-the-art; and lastly, Section 5 highlights the principal conclusions and future perspectives this research.

2. Data and methods

2.1. Observed wind speed data

Two observational datasets covering the 59-yr 1961–2019 period are used in this study: one corresponding to the monthly mean near-surface wind speed (SWS) and the other to the daily peak wind gust (DPWG). The datasets include records from 87 meteorological stations (77 in Spain and 10 in Portugal) distributed across the IP along with the Balearic Islands and Melilla (Fig. 1; Table S1 in Supplementary material). This means an increase of 11 and 7 stations with respect to the previous studies by Azorin-Molina et al. (2014) and Azorin-Molina et al. (2016), respectively. These datasets were supplied by the Spanish Meteorological Agency (AEMET) and the Portuguese Sea and Atmosphere Institute (IPMA). Azorin-Molina et al. (2014) already described the anemometer types used to measure SWS and DPWG. Along with these reported wind instruments, we noticed in the weather maintenance notes at AEMET the replacement of the SEAC SV5 anemometer with the Thies ultrasonic 2D and Thies first class anemometers in the automatic weather stations during the last two decades.

Both AEMET and IPMA measure DPWG as the maximum wind speed recorded as a 3-s mean over 24 h (WMO, 1987), while SWS is estimated from daily mean wind speed data averaged from standard 10-min mean observations at 07:00, 13:00, and 18:00 UTC by AEMET; and from hourly mean wind speed data when an automatic weather station (AWS) is used and from daily wind run data (*i.e.*, the total distance of the travel wind over 24 h) from 09:00 to 09:00 UTC by IPMA. Months with less than 26 days of observations are rejected and set as missing. More detailed information for observed SWS and DPWG can be found in Azorin-Molina et al. (2014) and Azorin-Molina et al. (2016), respectively.

2.2. Quality control and homogenization

As mentioned above, changes in the location or height of the anemometers, as well as their wear, can introduce spurious shifts in the wind series. To remove non-climatic artifacts, a robust quality control and homogenization process is carried out through the R package Climatol (available online at https://CRAN.R-project.org/package=climatol; last accessed December 16, 2021). This homogenization approach is similar to the one applied in the wind studies by Azorin-Molina et al. (2016, 2018b) and Zhang et al. (2020).

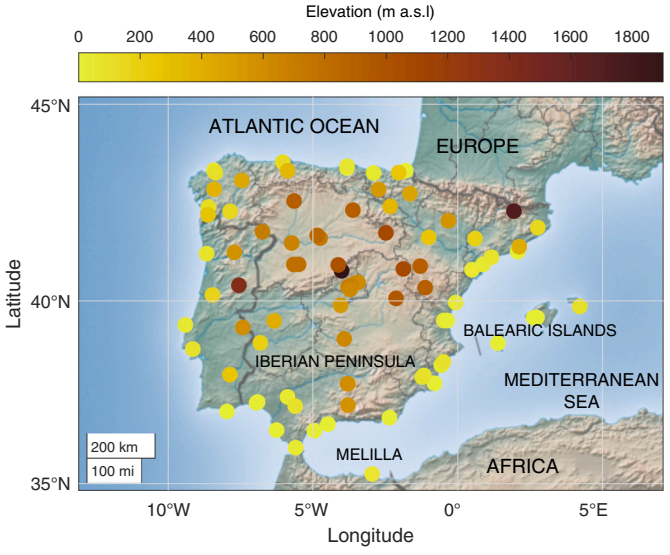

Fig. 1. Measurement locations of near-surface mean wind speed (SWS) and daily peak wind gust (DPWG) observations.

First, all series are normalised dividing them by their mean value of the entire period (*i.e.*, 1961–2019). Then, every single data in each series is estimated as an average of its nearest neighbours and the difference between the estimated and observed value is computed. If this difference exceeds a prescribed threshold, the corresponding value is discarded. The Standard Normal Homogeneity Test (SNHT; Alexandersson, 1986) is applied to the series of differences obtained; when the maximum SNHT value of the series exceeds a predefined threshold, the series is split. The process is applied iteratively until no value that exceeds both established thresholds is detected. Thresholds are chosen from the observation of the histograms of the maximum values of SNHT and of standardized anomalies. If there is no metadata available, a high threshold is chosen to avoid rejecting real extreme values, especially for DPWG. This is done at the cost of risking the presence of spurious extreme values.

Finally, the missing values were filled in with a weighted average of the four nearest observational values (in normalised form) available at each time step, assigning to each one a weight inversely proportional to the distance to the station considered. Climatol generated a homogenized and complete SWS and DPWG series, which is mandatory before assessing long-term wind speed changes (Azorin-Molina et al., 2014). A detailed example of the breakpoint detection and homogenization adopted in this research can be found in Azorin-Molina et al. (2018b, see Fig. 2 therein). In summary, this approach corrected 775 and 608 breakpoints for SWS and DPWG, respectively, and selected as homogeneous wind speed data from the original 87 wind series (77 in Spain and 10 in Portugal) as shown in Fig. 1 and Table S1 for 1961–2019.

2.3. Atmospheric circulation: teleconnection indices, weather types and computed parameters

To quantify the influence of atmospheric circulation changes on the observed SWS and DPWG, the following parameters are used:

The indices of three modes of climate variability: the North Atlantic Oscillation (NAO), the Mediterranean Oscillation (MO) and the Western Mediterranean Oscillation (WeMO) (Fig. 2). They were selected because they are responsible for much of the climate variability in the IP (Palutikov, 2003; Martin-Vide and Lopez-Bustins, 2006; Vicente-Serrano and Trigo, 2011). More specifically, Azorin-Molina et al. (2014) and Azorin-Molina et al. (2016) also examined their influence on wind speed variability for the same study area.

Two NAO indices are employed in order to add robustness to the results. The NAOi provided by the National Oceanic and Atmospheric Administration (NOAA; available online at https://www.cpc.ncep.noaa.gov/products/precip/CWlink/pna/nao.shtml; last accessed December 16, 2021) is obtained by applying a Rotated Principal Component Analysis technique to monthly standardized 500-mb geopotential height anomalies (Barnston and Livezey, 1987). A second NAOi provided by the Climate Research Unit (CRU; available online at https://crudata.uea.ac.uk/cru/data/nao/; last accessed December 16, 2021) is defined as the difference between the normalised sea level pressure over Gibraltar (36.1°N-5.3°W) and the normalised sea level pressure over Reykjavík (64.1°N-21.9°W) (Jones et al., 1997).

The MOi is provided by the CRU (available online at https://crudata.uea.ac.uk/cru/data/moi/; last accessed December 16, 2021). It is defined as the difference between the normalised sea level pressure over Gibraltar (36.1°N-5.3°W) and the normalised sea level pressure over Lod Airport (32.0°N-34.5°E) in Israel (Palutikov, 2003). It is proposed as a consequence of the dipole behaviour observed in the atmosphere in the region between the eastern and western Mediterranean basins (Criado-Aldeabuena and Soto-Navarro, 2013).

The WeMOi (available online at http://www.ub.edu/gc/es/wemo/; last accessed December 16, 2021) is calculated as the difference between the previously normalised sea level atmospheric pressures of the

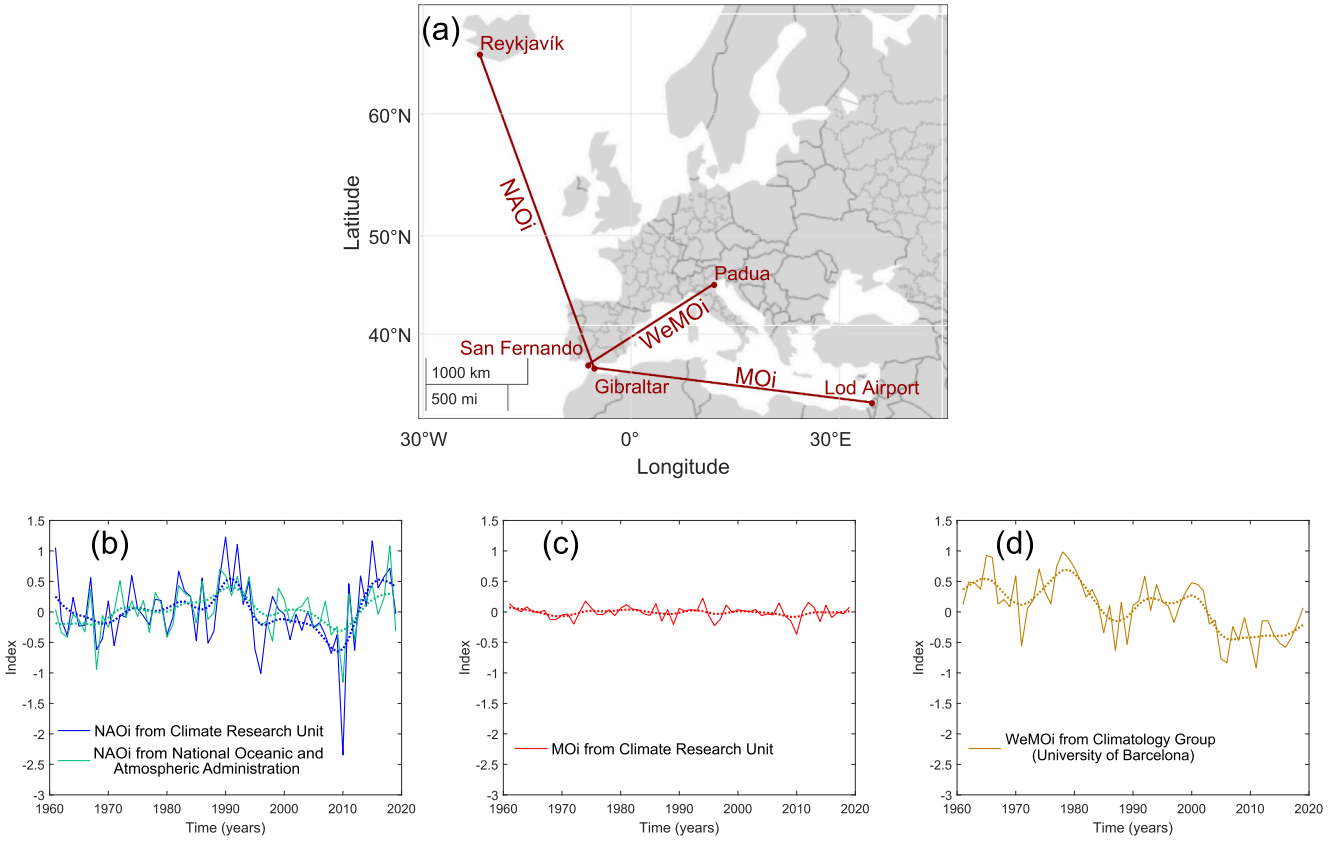

Fig. 2. (a) Transects of the teleconnection indices used in this work. Time series of (b) NAO index, (c) MO index and (d) WeMO index. The 10-year Gaussian low-pass filter is shown with a dotted thicker line to illustrate the multidecadal variability.

barometric dipole San Fernando (Spain, 36.5°N-6.2°W) and Padua (Italy, 45.4°N-11.9°E). The WeMOi was conceived because the precipitation in the east of the IP is weakly connected with the NAOi (Martin-Vide and Lopez-Bustins, 2006); this index is chosen since this could also be the case for the near-surface wind speed.

The Jenkinson and Collison scheme (hereinafter JC; Jenkinson and Collison, 1977) has been successfully applied in the IP before (*e.g.*, Azorin-Molina et al., 2016, and the references therein). It consists of assigning a synoptic weather type to each day based on seven circulation variables calculated from sea level pressure data. These types can be divided into: (i) directional flow types (N, NE, E, SE, S, SW, W, and NW); (ii) anticyclonic (A) and cyclonic (C) types; and (iii) hybrid types (AN, ANE, AE, ASE, AS, ASW, AW, ANW, CN, CNE, CE, CSE, CS, CSW, CW, and CNW). A more detailed description of the application of this method to the IP can be found in Azorin-Molina et al. (2011).

The methodology adopted was to calculate the number of days that a certain weather type occurred at the monthly, seasonal, and annual scale. In other words, we computed a time series for each weather type with its frequency (in days) of occurrence. Both the trends of each weather type and their correlations with the wind parameters defined in section 2.4 were calculated.

Four atmospheric parameters are calculated from the European Centre for Medium-Range Weather Forecasts reanalysis v5 (ERA5; Hersbach et al., 2019a, 2019b; Bell et al., 2020a, 2020b), in order to quantify atmospheric circulation changes in the study region that could influence the observed trends in SWS and DPWG. A similar procedure was applied in recent studies for explaining changes in DPWG in China (Zhang et al., 2020) and in Australia (Azorin-Molina et al., 2021). The source variables of these parameters are: the air temperature and dew point temperature at 500, 700 and 850 hpa levels, the zonal (u) and meridional (v) components of wind at 850 and 1000 hpa, the surface pressure and the geopotential at 850 hpa.

The four atmospheric parameters employed are: Pressure Gradient (PG), A index (A), Vertical Wind Shear (VWS) and Geostrophic Wind (V_g).

To assess how a change in the position or strength of the Hadley and Ferrel cells (Zurita-Gotor and Álvarez Zapatero, 2018) could have affected the observed SWS and DPWG changes, the spatial-average PG is computed between two regions that roughly correspond to the descending branch of the Hadley cell and the ascending one of the Ferrel cell. Both regions are in the longitudinal band of 25°W-15°E, but one is located at low latitude (LL; *i.e.*, 27.5°–32.5°N) and the other at high latitude (HL; *i.e.*, 57.5°–62.5°N). The PG is calculated as follows:

$$PG = \frac{\left(\sum_{i=1}^{n} PHL_i - \sum_{i=1}^{n} PLL_i\right)}{n}, \quad (1)$$

where n is the total number of longitude grid points and PHL_i and PLL_i are the near-surface air pressure on each longitude in the HL and LL, respectively. Grid points are regularly distributed along meridians and their number is latitude-independent.

The A index (A) gives an approximate measure of atmospheric thermal stability (Zhang et al., 2013). It is computed as:

$$A = (T_{850} - T_{500}) - [(T_{850} - Td_{850}) + (T_{700} - Td_{700}) + (T_{500} - Td_{500})], \quad (2)$$

where T and Td are the air temperature and dew-point temperature, respectively, in Kelvin. The subscripts indicate the 500 hPa, 700 hPa and 850 hPa levels.

The Vertical Wind Shear (VWS) is used in the anaysis due to its relationship with surface roughness (Stull, 1988) and with the vertical transport of atmospheric momentum. It is defined as:

$$VWS = \sqrt{(U_{850} - U_{1000})^2 + (V_{850} - V_{1000})^2}, \quad (3)$$

where U and V denote the zonal and meridional components of wind (in $m\,s^{-1}$), respectively. Again, the subscripts indicate the 850 hPa and 1000 hPa levels.

The Geostrophic Wind (V_g) is selected as it is the main component of wind, especially in the extratropics, as the mid-latitude IP. It is calculated as follows:

$$V_g = -\frac{1}{f}\frac{\Delta H}{\Delta d}, \quad (4)$$

where, f is the Coriolis frequency (s^{-1}) and ΔH is the geopotential difference ($m^2\,s^{-2}$) at 850 hpa with respect to a distance Δd (m).

2.4. Statistical methods

We analyse trends and correlations of three near-surface wind parameters: (a) the monthly mean SWS anomaly; (b) the monthly mean DPWG anomaly; and (c) the number of days in which the value of DPWG exceeds the 90^{th} percentile of the series considered (f_{90}(DPWG)). Anomalies are computed as deviations from the 1981–2010 climatological mean. Calculations are made at the station level and over an aggregated average series. In addition, the calculation is made on three different time scales: annual, monthly, and standard boreal seasons (winter, December, January, and February; spring, March, April, and May; summer, June, July, and August; and autumn, September, October, and November).

Subsequently, to determine the cease of the *stilling* and the possible beginning of the *reversal* phenomenon, an adjustment to a piecewise linear regression model (Muggeo, 2003, https://cran.r-project.org/web/packages/segmented/index.html; last accessed December 16, 2021) is applied to the three wind parameters mentioned above. The breakpoints at which the trends change its magnitude in the last decades are classified into three categories according to their statistical significance obtained from a Score test (Muggeo, 2016): significant at $\alpha = 0.05$, significant at $\alpha = 0.10$ and not significant at $\alpha = 0.10$.

The non-parametric Mann-Kendall's tau-*b* test (Kendall and Gibbons, 1990) is used to determine the statistical significance of the trends between the breakpoints detected by the regression model and for the whole 1961–2019 period. This test is modified to account for autocorrelation in the data (Hamed and Rao, 1998). Two levels of statistical significance are applied: $\alpha = 0.05$ and $\alpha = 0.10$, helping readers to evaluate wind speed trends from a "process and importance" perspective, instead of only a "statistically significant" perspective (Wasserstein et al., 1998; Nicholls, 2001; Azorin-Molina et al., 2014). The trends are calculated using linear regression and its magnitude is expressed in meter per second per decade ($m\,s^{-1}\,dec^{-1}$) for the SWS and DPWG anomalies or in days per decade ($days\,dec^{-1}$) for the events exceeding the 90th percentile.

For a more comprehensive study of the calculated trends, a running trend analysis (*e.g.*, Brunetti et al., 2010) is applied to accurately determine the onset and persistence of wind trends. The time windows width ranges from 10 years up to the length of the whole series (59 years).

The relationship between the SWS and DPWG parameters and the teleconnection indices or the JC scheme is quantified through the Spearman's rank correlation coefficient. The statistical significance of this correlation is assessed at the significance level of $\alpha = 0.05$.

Finally, magnitudes and statistical significance of the trends of the atmospheric circulation parameters defined in Section 2.3 are computed to relate them with those obtained in both the SWS and DPWG parameters. The units of these trends are dec^{-1} for the teleconnection indices, $days\,dec^{-1}$ for the weather types, $hPa\,dec^{-1}$ for the pressure gradient, $K\,dec^{-1}$ for the A index and $m\,s^{-1}\,dec^{-1}$ for the geostrophic wind and the vertical wind shear.

3. Results

3.1. The stilling and reversal phenomena across the IP

The decline in both SWS and DPWG during the second half of the 20th century is clearly noticeable in all timescales (Fig. 3), revealing the *stilling* phenomenon. The start of the most pronounced slowdown in winds occurred around 1978, with values remaining approximately constant or with a slight negative slope prior to that year. Fig. 3 also shows a greater inter-annual wind variability in winter than in summer, especially for monthly mean anomalies of both SWS and DPWG.

According to our results, the interruption of the *stilling* and a possible beginning of a weak *reversal* phenomenon occurred in the IP. However, the year of detection of the cessation of the *stilling* is not clearly determined, as it varies considerably among seasons and the three wind parameters (Table 1). For instance, it varied from as early as 1999 for SWS anomalies and f_{90}(DPWG) in winter, to 2018 for the three wind parameters in autumn. In summer, we did not detect any significant *reversal* and the *stilling* dominated until 2019. At the annual scale, we detect the onset year of the *reversal* close to 2007, being these breakpoints significant ($p < 0.05$) for SWS anomalies and f_{90}(DPWG). Since the year reported by Zeng et al. (2019) as the beginning of the global *reversal* is 2010, trends before and after this year have been calculated for comparison purposes.

Considering the entire period 1961–2019, the three wind parameters show significant ($p < 0.05$) negative trends for all seasons and at the annual scale (Table 2). When we focus on the period prior to 2010, the statistically significant negative trends remain for the three parameters on the annual scale and in winter, being stronger for the latter. For the rest of seasons, spring showed significant ($p < 0.05$) negative trends for SWS and DPWG anomalies and a not significant ($p < 0.10$) negative one for f_{90}(DPWG); in summer and autumn, the decline for SWS anomalies and f_{90}(DPWG) is significant ($p < 0.05$) and of lesser significance ($p < 0.10$) for DPWG anomalies. Conversely, the trends are not significant (p

Table 1
Annual and seasonal breakpoint years of (a) monthly mean SWS anomaly, (b) monthly mean DPWG anomaly and (c) number of days exceeding the 90th DPWG percentile (f_{90}(DPWG)) for the IP. Statistically significant breakpoints are shown in boldface for $p < 0.05$ and in italic for $p < 0.10$.

	(a)	(b)	(c)
Annual	**2007**	2006	**2006**
Winter (DJF)	1999	2000	1999
Spring (MAM)	2003	*2011*	*2015*
Summer (JJA)	–	–	–
Autumn (SON)	2018	2018	2018

Table 2
Annual and seasonal trends of (a) monthly mean SWS anomaly (in $m s^{-1} dec^{-1}$), (b) monthly mean DPWG anomaly (in $m s^{-1} dec^{-1}$) and (c) f_{90}(DPWG) (in $days dec^{-1}$) for the IP for 1961–2019, 1961–2010 and 2010–2019. Statistically significant trends are shown in boldface for $p < 0.05$ and in italic for $p < 0.10$.

		(a)	(b)	(c)
Annual	1961–2019	**−0.15**	**−0.15**	**−5.46**
	1961–2010	**−0.15**	**−0.16**	**−6.46**
	2010–2019	+0.04	−0.01	+7.82
Winter (DJF)	1961–2019	**−0.19**	**−0.28**	**−1.51**
	1961–2010	**−0.20**	**−0.33**	**−1.83**
	2010–2019	−0.06	−0.59	−0.73
Spring (MAM)	1961–2019	**−0.18**	**−0.17**	**−1.44**
	1961–2010	**−0.19**	**−0.21**	−1.80
	2010–2019	+0.21	+0.63	+7.94
Summer (JJA)	1961–2019	**−0.11**	**−0.06**	**−1.32**
	1961–2010	**−0.10**	*−0.05*	**−1.23**
	2010–2019	−0.03	−0.11	−0.30
Autumn (SON)	1961–2019	**−0.11**	**−0.09**	**−1.26**
	1961–2010	**−0.10**	*−0.06*	**−1.20**
	2010–2019	+0.05	+0.02	−1.45

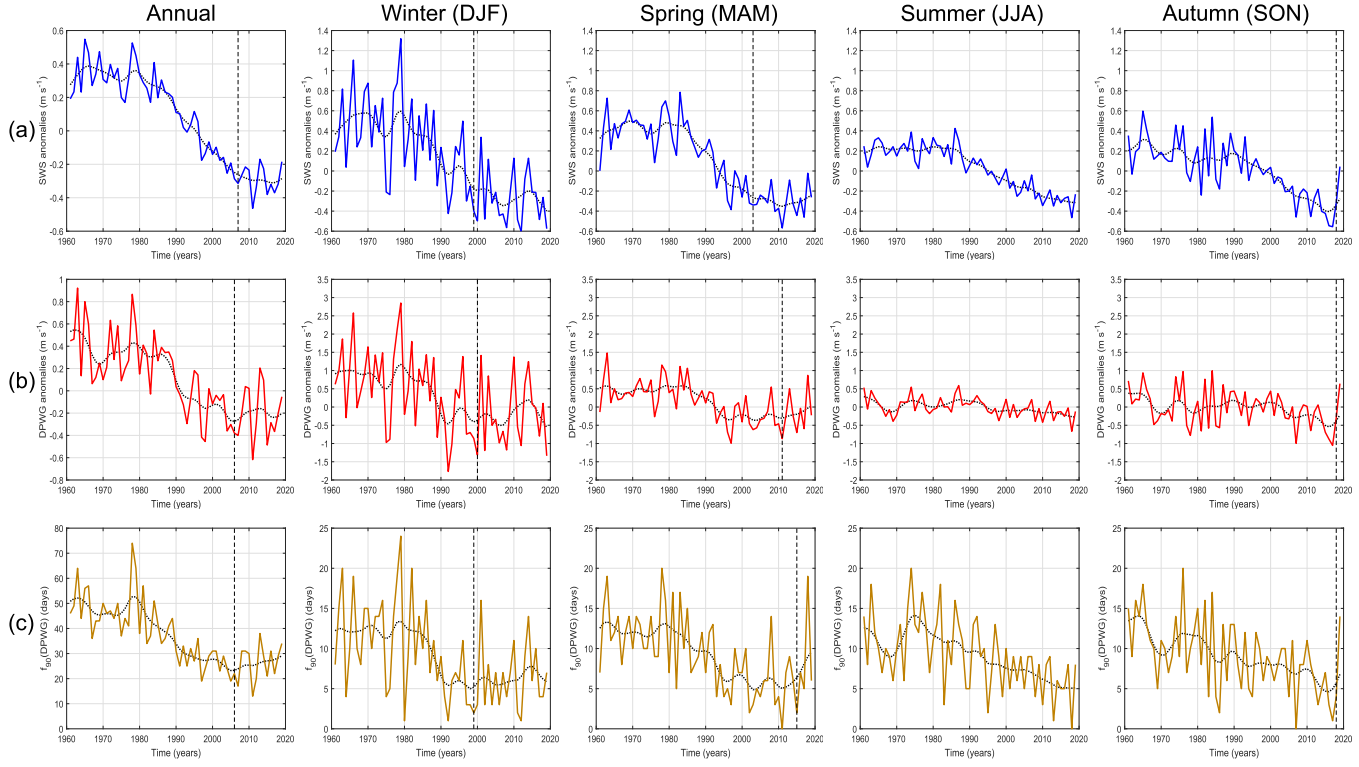

Fig. 3. Time series of (a) monthly mean SWS anomaly (in $m s^{-1}$), (b) monthly mean DPWG anomaly (in $m s^{-1}$) and (c) number of days exceeding the 90th DPWG percentile (f_{90}(DPWG)); in days) for the IP from 1961 to 2019. The 10-year Gaussian low-pass filter is shown with a black dotted line to illustrate the multidecadal variability. A vertical dashed line shows the onset of the *reversal* in each case when a breakpoint is detected ($p < 0.05$).

< 0.10) for 2010–2019. This is because of the quite short time-period and the high inter-annual variability. However, these trends are generally positive, or at least closer to zero when compared to the previous 1961–2010 period. These results suggest a break in the *stilling* and a possible occurrence of the *reversal* in the IP.

Analogous results to annual and seasonal scale are reported on a monthly scale (Table S2; Figs. S1–S3 in Supplementary material). In fact, trends are negative and statistically significant ($p < 0.05$) for almost every month and variable for the 1961–2019 and 1961–2010 periods, while trends are weaker or even become positive for 2010–2019. The *reversal* is not detected in July, August, and September.

The running trends analysis confirms the *stilling* phenomenon during the second half of the 20th century (Fig. 4). The *reversal* is also detected in winter and weakly observed in spring for window lengths <15–20 years, although these positive trends are not significant at $p < 0.05$. It is worth mentioning that since the minimum time window is 10 years, if the *reversal* phenomenon has begun in the last decade, it will not appear fully represented in this analysis, this occurs *e.g.*, in autumn. For window lengths of approximately 30 years or more, no positive trends are observed, which confirms the fact that the *reversal* would have occurred in recent decades and that it would be preceded by the *stilling* phenomenon. In addition, it is also remarkable the positive trends observed around 1970s in time windows of ~10–15 years, which reflects the marked inter-annual variability of winds as previous *reversal* cycles already occurred in the past.

Negative and statistically significant trends ($p < 0.05$) dominated across the IP in all seasons for 1961–2019 (Fig. 5); the *reversal* phenomenon is masked here as the spatial trends are computed for the entire study period. Only the northeast of the IP displays some statistically significant ($p < 0.05$) positive trends for DPWG anomalies in summer or non-significant trends in spring. Overall, the strongest magnitude of the declines occurs in winter and spring for SWS and DPWG anomalies, while the f_{90}(DPWG) shows a weak intra-annual variability. DPWG anomalies generally show a greater decline than SWS anomalies, which confirms that the *stilling* is more noticiable for stronger winds.

At the annual scale, larger magnitudes for f_{90}(DPWG) trends were expected compared to seasonal statistics due to the wider time range. For the same reason, annual and seasonal trends are greater than the monthly ones (Fig. S6 in Supplementary material). At this monthly scale, greatest decreases for the three wind variables occur for the winter and spring months, being smaller in the summer and autumn months (Figs. S4–S6 in Supplementary material). DPWG trends show great variability in the autumn months, alternating positive and negative trends throughout the territory, being mostly non-significant (Fig. S5 in Supplementary material).

3.2. Relationship between near-surface wind speed and atmospheric circulation

Table 3 shows the correlation between the three teleconnection indices and the three wind parameters for the IP. WeMOi exhibits the highest (positive) correlation at all scales, except for winter, where the negative correlations with NAOi and MOi are higher in absolute value than the positive ones computed for this index. All correlations with the WeMOi are statistically significant ($p < 0.05$) with the exception of summer for f_{90}(DPWG). Correlations at annual and spring scales stand out, reaching values higher than +0.60. Looking at the spatial distribution (Fig. 6), positive and statistically significant ($p < 0.05$) correlations dominate in most of the stations, with the southwest of the peninsula being practically the only area where statistically significant negative correlations appear. Similar results are found on a monthly scale (Figs. S17-S19 in Supplementary material). Table 4 shows the trend of the three indices for the three periods considered. Regarding

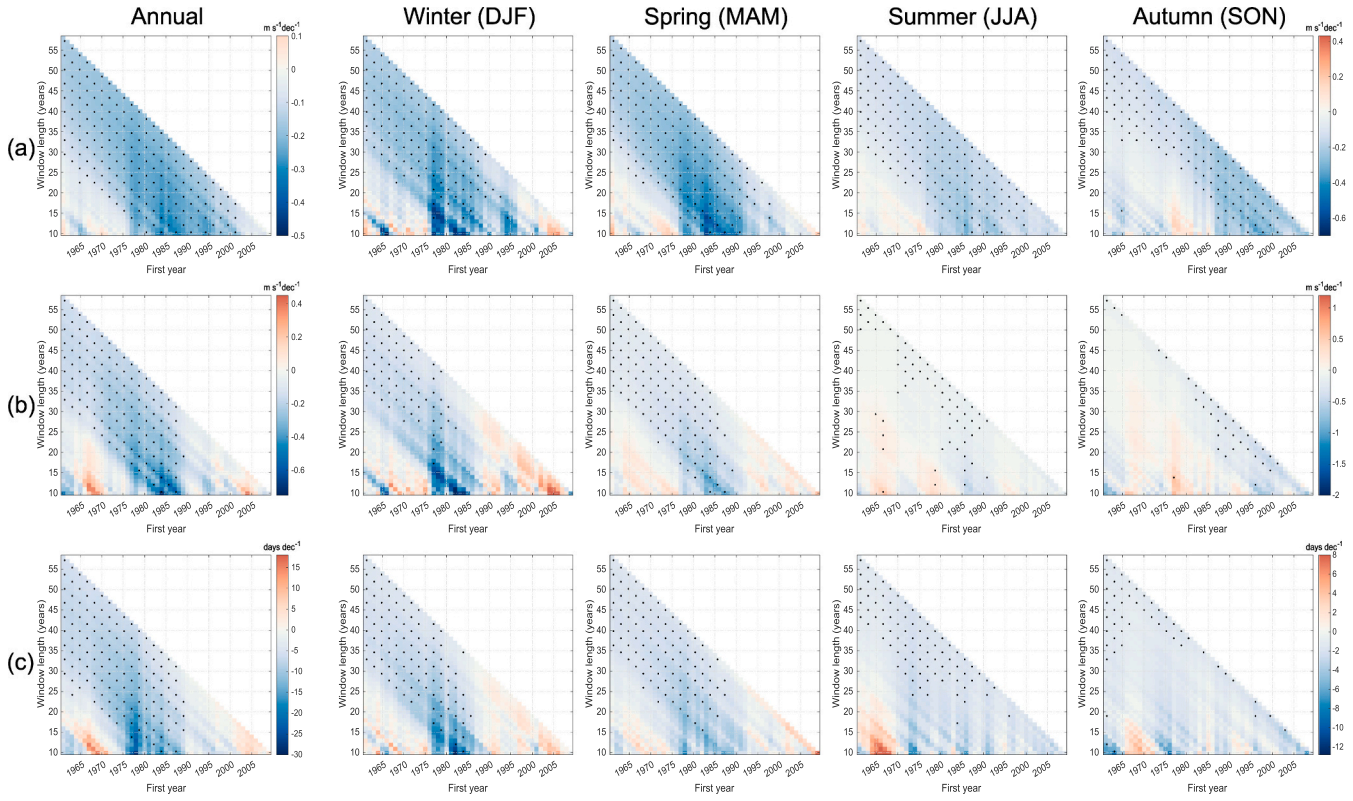

Fig. 4. Running trends analysis for (a) monthly mean SWS anomaly (in $m s^{-1} dec^{-1}$), (b) monthly mean DPWG anomaly (in $m s^{-1} dec^{-1}$) and (c) f_{90}(DPWG) (in $days dec^{-1}$). X-axis indicates the starting year of any temporal window over which the trend is calculated and Y-axis represents the window length. Black dots indicate significant trends at $p < 0.05$. Different scales have been used for each variable in order to appreciate trends.

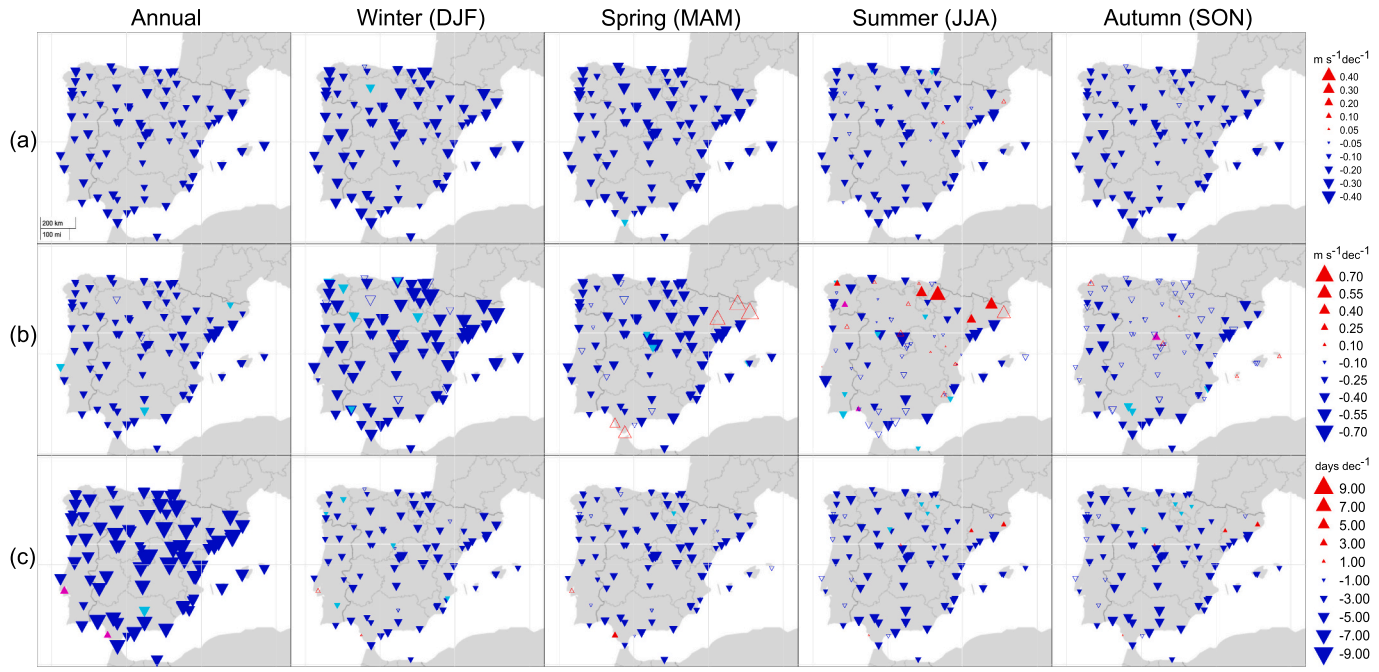

Fig. 5. Annual and seasonal spatial distribution of the sign, statistical significance and magnitude of trends of (a) monthly mean SWS anomaly (in $m s^{-1} dec^{-1}$), (b) monthly mean DPWG anomaly (in $m s^{-1} dec^{-1}$) and (c) f_{90}(DPWG) (in $days dec^{-1}$) for the homogenized series of the 87 stations for 1961–2019. Blue and red filled triangles are significant at $p < 0.05$; cyan and magenta filled triangles are significant at $p < 0.10$; and non-filled triangles are non-significant at $p < 0.10$. Different scales have been used for each variable in order to appreciate trends.

Table 3
Annual and seasonal Spearman's rank correlation coefficients between the three teleconnection pattern indices used and (a) monthly mean SWS anomaly, (b) monthly mean DPWG anomaly and (c) f_{90}(DPWG) for 1961–2019. Statistically significant Spearman's rank correlation coefficients are shown in boldface for $p < 0.05$.

		(a)	(b)	(c)
Annual	NAOi	−0.07	−0.09	−0.02
	MOi	0.00	−0.05	−0.01
	WeMOi	**+0.66**	**+0.50**	**+0.58**
Winter (DJF)	NAOi	**−0.42**	**−0.47**	**−0.34**
	MOi	**−0.47**	**−0.51**	**−0.42**
	WeMOi	**+0.31**	**+0.35**	**+0.33**
Spring (MAM)	NAOi	−0.14	−0.20	−0.15
	MOi	+0.18	+0.03	+0.11
	WeMOi	**+0.66**	**+0.61**	**+0.64**
Summer (JJA)	NAOi	+0.13	−0.06	+0.01
	MOi	+0.19	+0.12	**+0.32**
	WeMOi	**+0.33**	+0.17	+0.25
Autumn (SON)	NAOi	+0.02	−0.23	+0.01
	MOi	+0.03	−0.19	−0.03
	WeMOi	**+0.37**	**+0.27**	**+0.33**

WeMOi, a decrease is observed on all time scales for the periods 1961–2010 and 1961–2019, in most cases statistically significant ($p < 0.05$). Around 2010, trends changed and became positive, although these are not statistically significant. This trend behaviour is most pronounced in spring, is diluted on an annual scale and does not happen in summer.

Given that the time series of the NAOi extracted from the CRU and NOAA practically overlap (Fig. 2(b)), and since the results achieved are very similar for both indices, here we only present the results from the CRU index (results from NOAA can be found in the supplementary material; Figs. S7–S10 and Tables S3–S6). The highest correlation between the NAOi and the three wind parameters occurs in winter, being negative and significant ($p < 0.05$) and reaching values up to −0.50. No other significant correlations are found in the other seasons or at the annual scale (Table 3). Almost all stations show a statistically significant ($p < 0.05$) negative correlation between NAOi and the three wind parameters in winter (Figs. 7 and S7 in Supplementary material). For the rest of the seasons, the correlations are of smaller magnitude and fewer stations show statistical significance, with summer showing the highest number of positive correlations, especially in June (Figs. S8-S13 in Supplementary material). On an annual scale, there is no correlation. The trends observed in the NAOi series show a lower statistical significance compared to those of the WeMOi (Table 4), probably due to the higher interannual variability of the NAOi (Fig. 2). The only statistically significant at $p < 0.05$ trends are in spring and summer for the 1961–2010 period. In winter, the statistically significant ($p < 0.10$) positive trend in the 1961–2019 period would be consistent and could be related to the observed decrease in the wind parameters for the same period.

The correlations between MOi and wind parameters follow a similar pattern to that observed for NAOi (Table 3), being negative and statistically significant ($p < 0.05$) in winter, of lesser magnitude and significance in the rest of the seasons and closed to zero at the annual scale. This pattern remains the same when considering the spatial distribution of the correlations (Fig. 8 and S14-S16 in Supplementary material). However, it is worth mentioning a difference between these two indices, observed both in the spatial distribution (Figs. 7 and 8) and for the IP as a whole (Table 3); while for NAOi negative correlations are dominant in spring and summer, in the case of MOi the sign is reversed. MOi trends are generally smaller compared to those of the other two indices (Table 4), there is a significant ($p < 0.05$) slight decline in spring and summer for 1961–2019 and 1961–2010, which is maintained on an annual scale for the second period. As well as for NAOi, a statistically significant ($p < 0.10$) positive trend appears in winter for 1961–2019.

Fig. 9 shows the correlation between the frequency of occurrence of each weather type of the JC scheme and each wind parameter on a monthly scale. The weather types that present the highest positive and statistically significant ($p < 0.05$) correlations are the W and NW types, for all months except in July and August. On the contrary, the stable A circulations weaken winds and showed the highest negative correlations

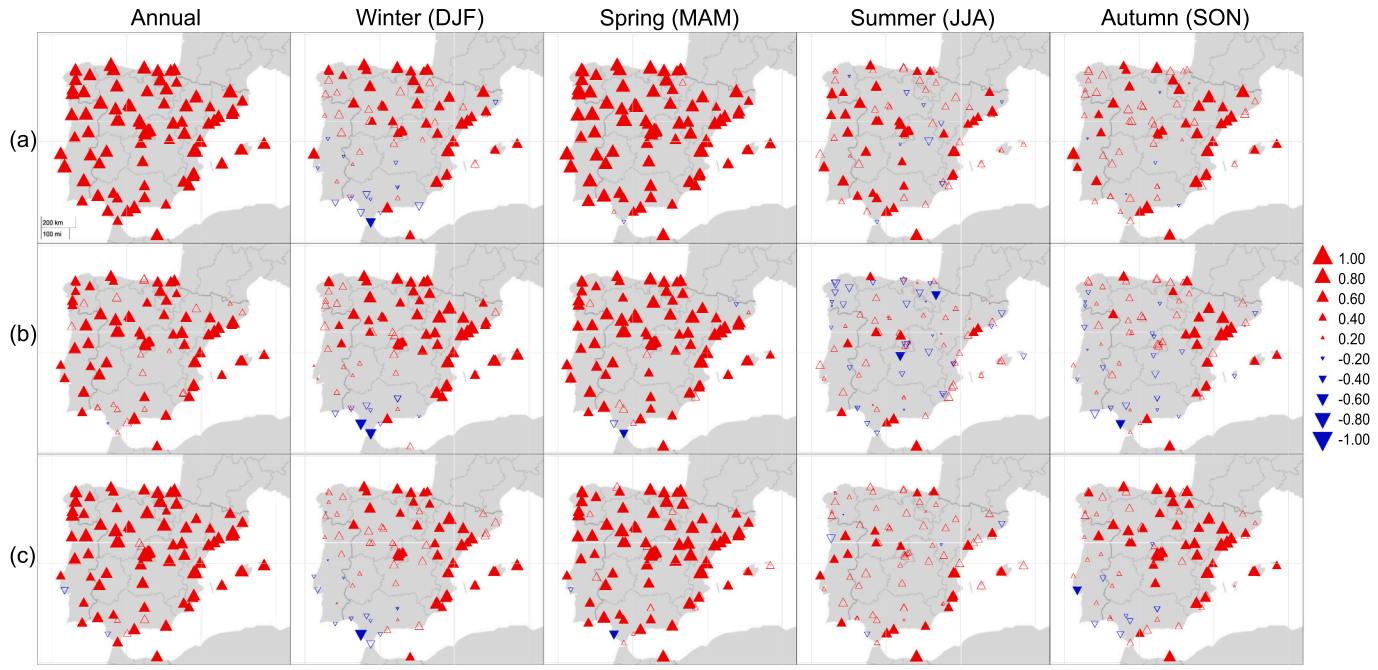

Fig. 6. Spatial distribution of the sign, magnitude and statistical significance of Spearman's rank correlation coefficients (r) between WeMO index and (a) monthly mean SWS anomaly, (b) monthly mean DPWG anomaly and (c) f_{90}(DPWG) at annual and seasonal time scales for 1961–2019. Filled triangles are significant at $p < 0.05$ and non-filled triangles are non-significant at $p < 0.05$.

Table 4
Annual and seasonal trends (in dec^{-1}) of the (a) NAO index from CRU, (b) MO index and (c) WeMO index for 1961–2019, 1961–2010 and 2010–2019. Statistically significant trends are shown in boldface for $p < 0.05$ and in italic for $p < 0.10$.

		(a)	(b)	(c)
Annual	1961–2019	−0.01	−0.01	**−0.16**
	1961–2010	−0.11	**−0.01**	**−0.15**
	2010–2019	+1.76	+0.17	+0.44
Winter (DJF)	1961–2019	*+0.19*	*+0.04*	−0.04
	1961–2010	+0.09	+0.01	**−0.13**
	2010–2019	+3.33	+0.65	+0.16
Spring (MAM)	1961–2019	+0.05	**−0.03**	**−0.27**
	1961–2010	−0.05	**−0.02**	**−0.27**
	2010–2019	+2.23	+0.15	+0.71
Summer (JJA)	1961–2019	*−0.15*	**−0.02**	**−0.17**
	1961–2010	**−0.22**	**−0.02**	−0.07
	2010–2019	+1.82	−0.13	−0.05
Autumn (SON)	1961–2019	*−0.14*	−0.02	**−0.17**
	1961–2010	**−0.23**	−0.02	*−0.14*
	2010–2019	+0.77	+0.27	+0.90

with SWS and DPWG, particularly from October to February when these correlations are statistically significant ($p < 0.05$). In July and August, no synoptic type shows significant correlation with the wind parameters. The weather types with the highest correlation with the three wind parameters on an annual and seasonal scale for the IP are presented in Table 5. The highest correlations, both positive (type W) and negative (type A), occur in winter, and all of them are statistically significant ($p < 0.05$). In autumn and spring, the statistical significance is maintained but the values decrease; the maximum positive correlations alternate between the W, N and NW types, while the maximum negative correlations occur with the SE type in spring and with the E type in autumn. In summer, the maximum negative correlations with the ASW and CSE types maintain statistical significance, whereas the maximum negative correlations with the CN and CW types lose it. In winter, the positive correlations are greater in absolute value than the negative ones, being the opposite for the rest of seasons. On an annual scale, the positive correlation with the W type is not significant ($p < 0.05$) for SWS anomalies but it is significant for DPWG anomalies and for f_{90}(DPWG), as is the case with the negative correlations with the A type. It is noteworthy that the correlations with the parameters dependent on gusts, DPWG anomalies and f_{90}(DPWG), are higher in absolute value compared to those corresponding to the mean wind. Table 6 shows the trends of the frequency of occurrence of each of the weather types that most correlate with the wind parameters, which were determined in Table 5. The *stilling* phenomenon on annual scale may be associated with a decrease of the W type and an increase of the A type, even though weak statistical significance is found in these trends. Similar results are found in winter, in this case with statistical significance ($p < 0.05$) for 1961–2019. In spring, the statistically significant increase of the SE type in the 1961–2010 and 1961–2019 periods could be related to the *stilling* phenomenon, while the significant increase of the W type for 2010–2019 could be associated with the *reversal* phenomenon.

The HL-LL pressure gradient (*PG*; Eq. (1)) maintains a constant value within its own interannual variability, so no statistically significant ($p < 0.05$ or $p < 0.10$) trends are observed on seasonal scale (Fig. 10). The only exception would be winter for 1961–2019, where the negative and significant ($p < 0.05$) observed trend could be related to the *stilling* phenomenon. The decrease is maintained on an annual scale over the same period, being significant at $p < 0.10$ in this case.

A trend analysis of the A index (Eq. (2)) shows a decrease across most of the study region at the annual and seasonal scale for the three periods analysed (Fig. 11). The decline is more pronounced in winter in all three periods and of lesser magnitude for the rest of seasons, with positive trends appearing in some regions of the peninsula in summer and autumn for 2010–2019; in any case, trends are not significant ($p < 0.05$) across the IP. At the annual scale, the negative tendencies are statistically significant ($p < 0.05$) for the entire IP during 1961–2019, for most of it in the 1961–2010 period and not significant at any point of the region for 2010–2019.

Both vertical wind shear (Eq. (3); Fig. 12) and geostrophic wind (Eq. (4); Fig. 13) show similar patterns in the trends. In winter, they are negative in the latitudinal range where the IP is located, as well as south of it, and positive to the north, especially in the latitudinal range where

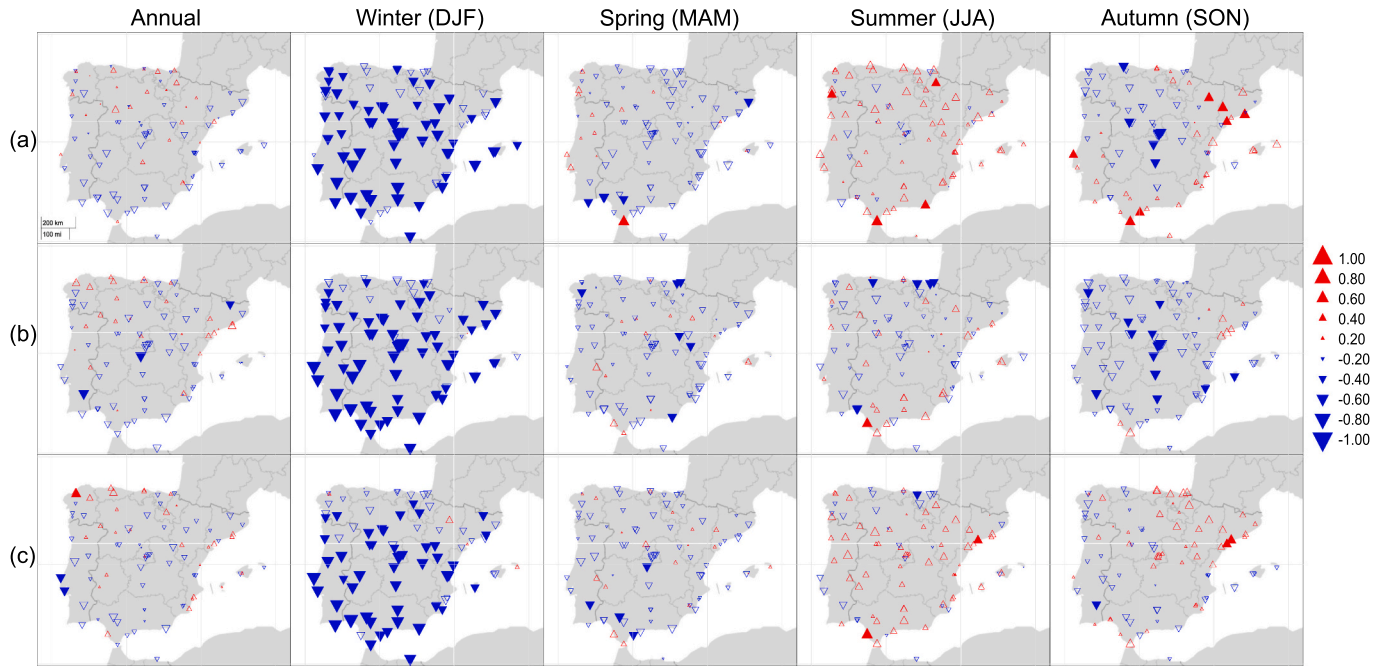

Fig. 7. Same as Fig. 6 but for the NAO index from CRU.

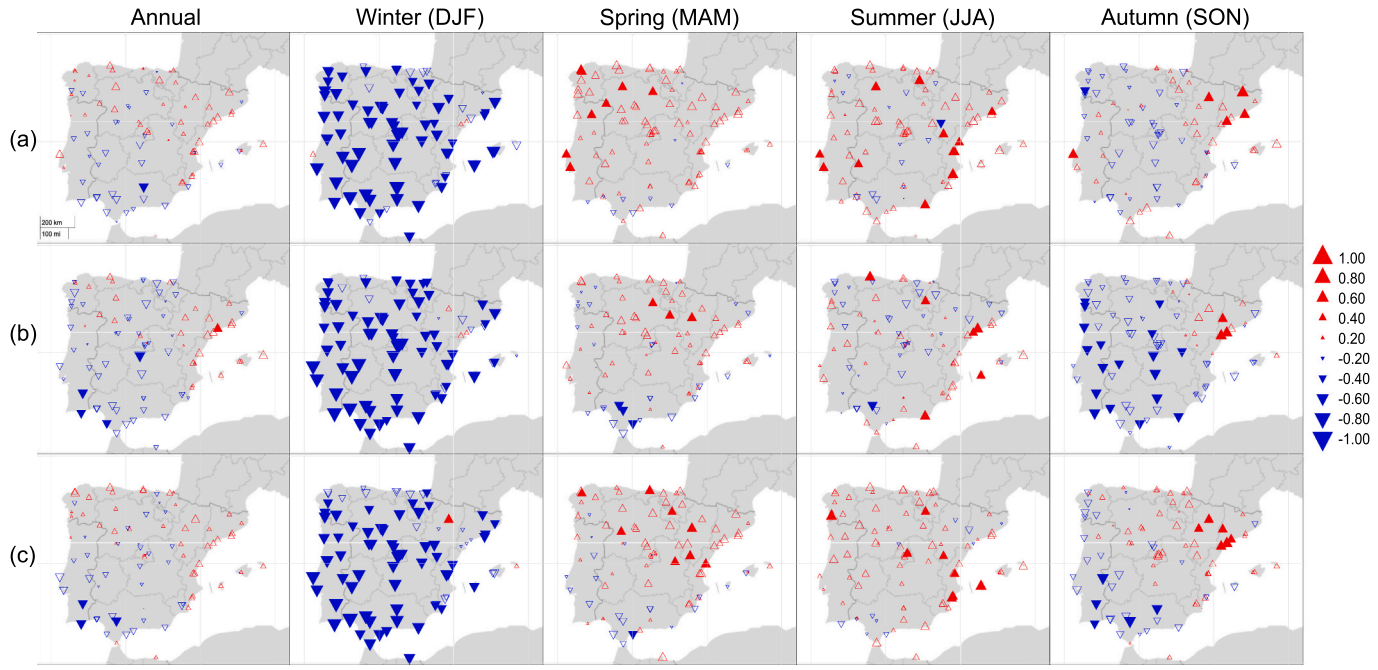

Fig. 8. Same as Fig. 6 but for the MO index.

Great Britain is situated. At the annual scale, the pattern is similar but smaller in magnitude. For the rest of seasons, the trends are of lesser magnitude than in winter and the pattern observed in that season disappears in most cases. If we focus on the IP, in most cases the trends are negative, with positive values appearing in some small regions in spring for 2010–2019 and in all periods for summer and autumn. In both parameters, most trends over the IP are not statistically significant ($p < 0.05$) in any of the periods analysed, whether on annual or seasonal scale.

4. Discussion

A spatiotemporal trend analysis of quality controlled and homogenized near-surface wind speed (SWS) and daily peak wind gust (DPWG) observations across the Iberian Peninsula (IP) has been revisited for 1961–2019, with the ultimate aim of identifying the recent *reversal* phenomenon reported by Zeng et al. (2019) after decades of *stilling* across this region (Azorin-Molina et al., 2014, 2016). At the same time, an analysis of the influence of atmospheric circulation drivers on the observed trends have been assessed.

Even though both the trends and correlations of wind parameters with the teleconnection indices and the JC scheme are partly consistent

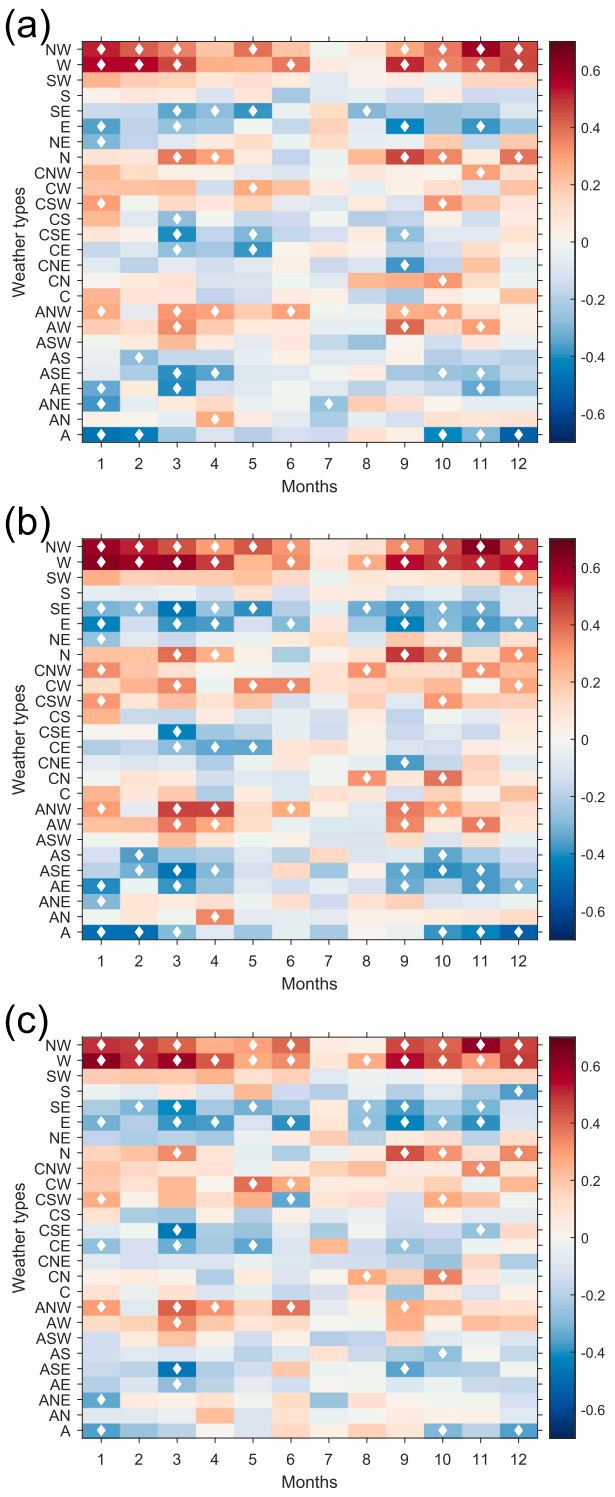

Fig. 9. Monthly Spearman's rank correlation coefficients between the 26 JC weather types and (a) monthly mean SWS anomaly, (b) monthly mean DPWG anomaly and (c) f_{90}(DPWG) for 1961–2019. White diamonds indicate significant correlation at $p < 0.05$.

with the previous studies by Azorin-Molina et al. (2014, 2016), the present work with longer anemometer time series has identified important differences concerning the magnitude. These differences seem related to the implementation of a slightly different approach in the quality control and homogenization process, which impacts on the resultant adjusted series (Brázdil et al., 2017). In addition, it should be noted that the number of stations has slightly increased compared to

Table 5
Maximum annual and seasonal Spearman's rank correlation coefficients between the correspondant JC type and (a) monthly mean SWS anomaly, (b) monthly mean DPWG anomaly and (c) f_{90}(DPWG) for 1961–2019. Statistically significant Spearman's rank correlation coefficients are shown in boldface for $p < 0.05$.

		JC	+R	JC	-R
Annual	(a)	W	0.30	A	−0.22
	(b)	W	**0.35**	A	**−0.38**
	(c)	W	**0.35**	A	**−0.30**
Winter (DJF)	(a)	W	**0.64**	A	**−0.50**
	(b)	W	**0.72**	A	**−0.55**
	(c)	W	**0.72**	A	**−0.46**
Spring (MAM)	(a)	N	**0.31**	SE	**−0.39**
	(b)	N	**0.45**	SE	**−0.46**
	(c)	W	**0.44**	SE	**−0.49**
Summer (JJA)	(a)	CN	0.11	ASW	**−0.31**
	(b)	CW	0.27	ASW	**−0.28**
	(c)	CW	0.21	CSE	**−0.29**
Autumn (SON)	(a)	NW	**0.32**	E	**−0.41**
	(b)	NW	**0.48**	E	**−0.43**
	(c)	NW	**0.37**	E	**−0.46**

previous studies, as mentioned in Section 2.1. Although this issue probably has less impact in the results, since the new stations are close to those that were already in use, a denser stations network improves the robustness of the conclusions. With all these in mind, the most remarkable difference compared to the previous studies is that Azorin-Molina et al. (2014, 2016) found a marked seasonality in the SWS and DPWG trends, with a dominance of declining trends in winter-spring and increasing ones in summer and autumn; with a noticeable monthly transition for DPWG. This seasonal cycle is not observed here, except in the NE of the IP. It is possible that the increase in winds detected over the NE Iberian Peninsula is associated with the synoptic atmospheric regimes only affecting this region, such as the Cierzo (Jiménez et al., 2008), the Tramontana and the Mistral (Obermann-Hellhund et al., 2018), so there would be no relation between this increase and the one detected across the whole IP by Azorin-Molina et al. (2014, 2016). A future assessment of wind changes from a regionalization approach would strongly help to better understand the mechanisms explaining the wind trends and variability.

The characteristics of the *stilling* phenomenon found in this work for the IP are consistent with those reported in previous wind studies on a global and regional scale. In fact, the negative trend of $-0.15\,m\,s^{-1}\,dec^{-1}$ reported in this work for SWS is in agreement with the range of downward trends reviewed by McVicar et al. (2012a), *i.e.*, between $-0.09\,m\,s^{-1}\,dec^{-1}$ and $-0.17\,m\,s^{-1}\,dec^{-1}$ depending on the threshold value imposed to the regional studies for the number of stations and the length of record. Furthermore, DPWG generally show a greater decline than SWS in winter and spring, which confirms that the *stilling* is more marked for strongest winds (Vautard et al., 2010). Lastly, the fact that *stilling* began in the 1970s and was preceded by a period of weak trends agrees with previous works (*e.g.*, Zhang and Wang, 2020).

It is worth noting that there is a large dispersion in the years for which a break in the *stilling* and an onset of the *reversal* is reported in the literature, both at the annual and seasonal scale. This might be related either to the calculation approach taken to identify the onset years, data issues (length of records, network densities, quality control and homogenization protocols) or actual regional differences. In addition, the fact that many parts of the world lack of an accurate study, prevents us from identifying geographic patterns at a wider scale. Considering the available studies, at the annual scale the years reported are: 2003 in Korea (Kim and Paik, 2015), 2001 in Saudi Arabia (Azorin-Molina et al., 2018b), 1992 in northwest China (Li et al., 2018), 2004 in the whole of China (Zhang and Wang, 2020), and 2010 globally, being between 2002 and 2011 for the random sets of stations resampled (Zeng et al., 2019). Most studies indicate the same onset year for the reversal on a seasonal

Table 6
Annual and seasonal trends (in days dec^{-1}) of the frequency of occurrence of the correspondant JC type obtained in Table 5 for 1961–2019, 1961–2010 and 2010–2019. Statistically significant trends are shown in boldface for $p < 0.05$ and in italic for $p < 0.10$.

		JC	T(+R)	JC	T(−R)	JC	T(+R)	JC	T(−R)
Annual	1961–2019	W	−0.36	A	1.33	–	–	–	–
	1961–2010	W	−0.44	A	1.98	–	–	–	–
	2010–2019	W	2.18	A	10.79	–	–	–	–
Winter (DJF)	1961–2019	W	**−0.42**	A	**1.59**	–	–	–	–
	1961–2010	W	−0.57	A	*1.58*	–	–	–	–
	2010–2019	W	−5.27	A	*16.12*	–	–	–	–
Spring (MAM)	1961–2019	W	−0.10	SE	**0.79**	N	−0.11	–	–
	1961–2010	W	−0.27	SE	**0.53**	N	−0.11	–	–
	2010–2019	W	**4.55**	SE	−4.42	N	4.48	–	–
Summer (JJA)	1961–2019	CN	−0.10	ASW	0.06	CW	−0.01	CSE	0.11
	1961–2010	CN	−0.15	ASW	0.06	CW	0.08	CSE	0.19
	2010–2019	CN	−0.24	ASW	0.00	CW	0.00	CSE	0.79
Autumn (SON)	1961–2019	NW	−0.12	E	*0.80*	–	–	–	–
	1961–2010	NW	0.09	E	0.82	–	–	–	–
	2010–2019	NW	−0.06	E	**7.76**	–	–	–	–

scale as on an annual scale; Zeng et al. (2019) is the only one to report different years depending on the season, although they range from 2009 to 2010 so they are almost the same as on an annual scale. The breakpoints found in this work are within the range of years reported by these previous studies both at the annual and seasonal scale, although seasonal differences were found. It is remarkable that the reversal did not occur in summer in the IP, although *e.g.,* Zha et al. (2019) also detected this phenomenon only in certain seasons. In autumn, there is a limitation in detecting the *reversal* as it occurs at the end of the series (2018), we could be more certain of its occurrence with a longer period of observations. The increasing rate of mean annual surface wind speed obtained by Zeng et al. (2019) worldwide for 2010–2017 is $+0.24\,m\,s^{-1}\,dec^{-1}$. This value would be within the confidence interval ($\alpha = 0.05$) of the trend calculated in this work for the annual mean wind speed anomaly for 2010–2019. Nonetheless, the trend period is very short and will be highly influenced by the inter-annual variability observed in the series, thus preventing the trends from being significant. Therefore, it is probably early to draw definitive conclusions and with a longer period of observations we could be more certain of the occurrence of the *reversal* phenomenon.

Given the significant positive correlation found between the wind parameters and the WeMOi, the negative trend found for this index before 2010 and the positive trend found after this year could be related to the *stilling* and *reversal* phenomena, albeit more studies are needed to attribute the physical processes behind. Additionally, the fact that the WeMOi has a broadly higher correlation with the wind parameters than the MOi might be due to the geographical complexity of the Mediterranean basin that could produce a distinction between the climate variability of its eastern fringe and the western one and could even decouple them (*e.g.*, Finné et al., 2019; Pisano et al., 2020). The ability of the NAOi to explain climate variability in Europe, especially in winter, is well known and has been extensively studied in the literature (*e.g.*, Pinto and Raible, 2012, and the references therein). However, a future use of the winter NAO flavours proposed by Rousi et al. (2020) could shed light on the mechanisms that may have triggered the *stilling* and *reversal* phenomena in the European region, as they offer more information than the typical NAO+ and NAO- classification.

When the influence of the Azores anticyclone reaches the IP calm days occur in the region, which explains the negative correlation of type A with wind parameters; at the same time, the positive correlations found with W and NW types are reasonable due to the influence of the jet stream that governs the atmospheric state in the study region (García-Valero et al., 2012). Conversely, the weakening of the correlations between wind parameters and weather types in summer could be due to the loss of strength of the synoptic atmospheric circulation (*i.e.*, northward displacement of westerlies) in favour of local to mesoscale phenomena such as sea breezes and local winds across the IP (Azorin-Molina et al., 2011), as previously discussed by Azorin-Molina et al. (2016). The trends reported here for the weather type occurrences agree with previous studies. In particular, Otero et al. (2018) found an increase for both type A and eastern types and a decrease in type W over southwest Europe, and an increase in type W over northern and central Europe.

Three of the results achieved in this study could be explained by a northward displacement of the eddy-driven jet (Barnes and Polvani, 2013) and could have had a direct influence on the *stilling* phenomenon. These are: (i) the decrease and increase in the frequency of occurrence of type W and A, respectively; (ii) the decrease of geostrophic winds and the VWS in the latitudinal strip occupied by the IP; and (iii) the increase of both atmospheric drivers in a strip north of it. In turn, this change in the jet stream could be caused by the expansion of the tropics detected in recent decades. This signal is robust and consistent across reanalyses and climate models, its causes are very diverse and may even depend on the metric considered (Davis and Birner, 2017). The internal variability of the climate system seems to be the fundamental factor driving this expansion, especially in the northern hemisphere (Grise et al., 2019); mainly through changes in sea surface temperature (SST) patterns, largely related to phenomena such as El Niño (ENSO) or the Pacific Decadal Oscillation (PDO) (Mantsis et al., 2017). The expansion of the tropics in recent decades would be associated with a pattern similar to that obtained during La Niña and a negative PDO (Allen and Kovilakam, 2017), although to explain the expansion as a whole, coupled atmosphere-ocean variability would not be sufficient and internal atmospheric variability would also have to be considered (Grise et al., 2019). There are differences in the expansion between hemispheres in terms of magnitude, seasonality, the physical mechanisms that trigger it, and even differences in the zonal distribution of this expansion (Watt-Meyer et al., 2019) that could explain the regional differences observed in the *stilling* and *reversal* phenomena. Moreover, both the decrease in VWS and the increase in the A index could be caused by an increase in atmospheric stability in response to global warming, which would imply a decrease in wind speed. This hypothesis has already been suggested in previous works that have studied this variable at a regional level in China (Zhang et al., 2020) and Australia (Azorin-Molina et al., 2021). Increased surface roughness has been previously proposed as a possible

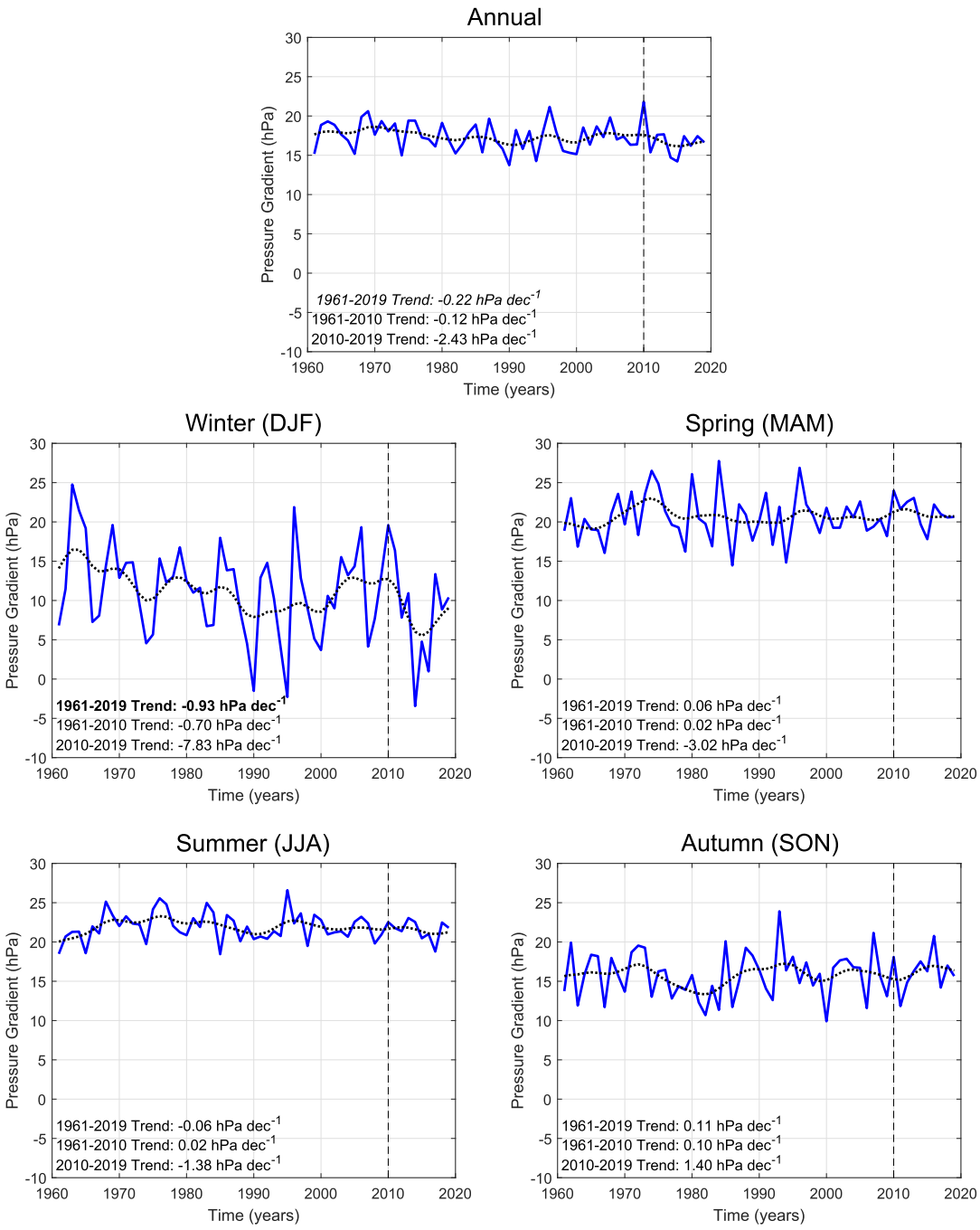

Fig. 10. Time series of the surface pressure gradient parameter (denoted PG; in hPa) from 1961 to 2019. The 10-year Gaussian low-pass filter is shown with a black dotted line to illustrate the multidecadal variability. A vertical dashed line shows the 2010 year. Decadal trends (in hPa dec^{-1}) are also displayed in each plot for the three periods considered; statistically significant trends are shown in boldface for $p < 0.05$ and in italic for $p < 0.10$.

cause of the *stilling* phenomenon (*e.g.*, Vautard et al., 2010; Zeng et al., 2018; Zhang et al., 2019). In this work, VWS has been analysed for its relationship with surface roughness (Stull, 1988). An increase in surface roughness would lead to an increase in VWS due to a decrease in surface wind speed. However, the results show the opposite, this may be due to the decrease in wind speed at high levels counteracting what is occurring at low levels.

The study of the atmospheric circulation changes carried out in this work identifies the WeMO as the most suitable mode of climate variability to have an impact over the *reversal* phenomenon in the IP. From the analysis of the running trends, it seems that the *reversal* is part of the internal variability of the surface winds, which agrees with the role played by the ocean-atmosphere oscillations in modulating wind changes as discussed by Zeng et al. (2019). Not having sufficiently long series to observe these cycles would have caused them to go unnoticed. This has recently been explored by Wohland et al. (2021), where it is mentioned that the wind trends produced by the internal variability of the climate system are one order of magnitude larger than those produced by forced changes. Nevertheless, the uncertainty is still large, studies such as the one recently published by Zhang et al. (2021) claim that simulations with only natural climate forcing agents do not accurately capture the observed wind speed changes and therefore all forcing simulations are needed, at least when the region under consideration is northern China. The lack of long instrumental wind speed series beyond

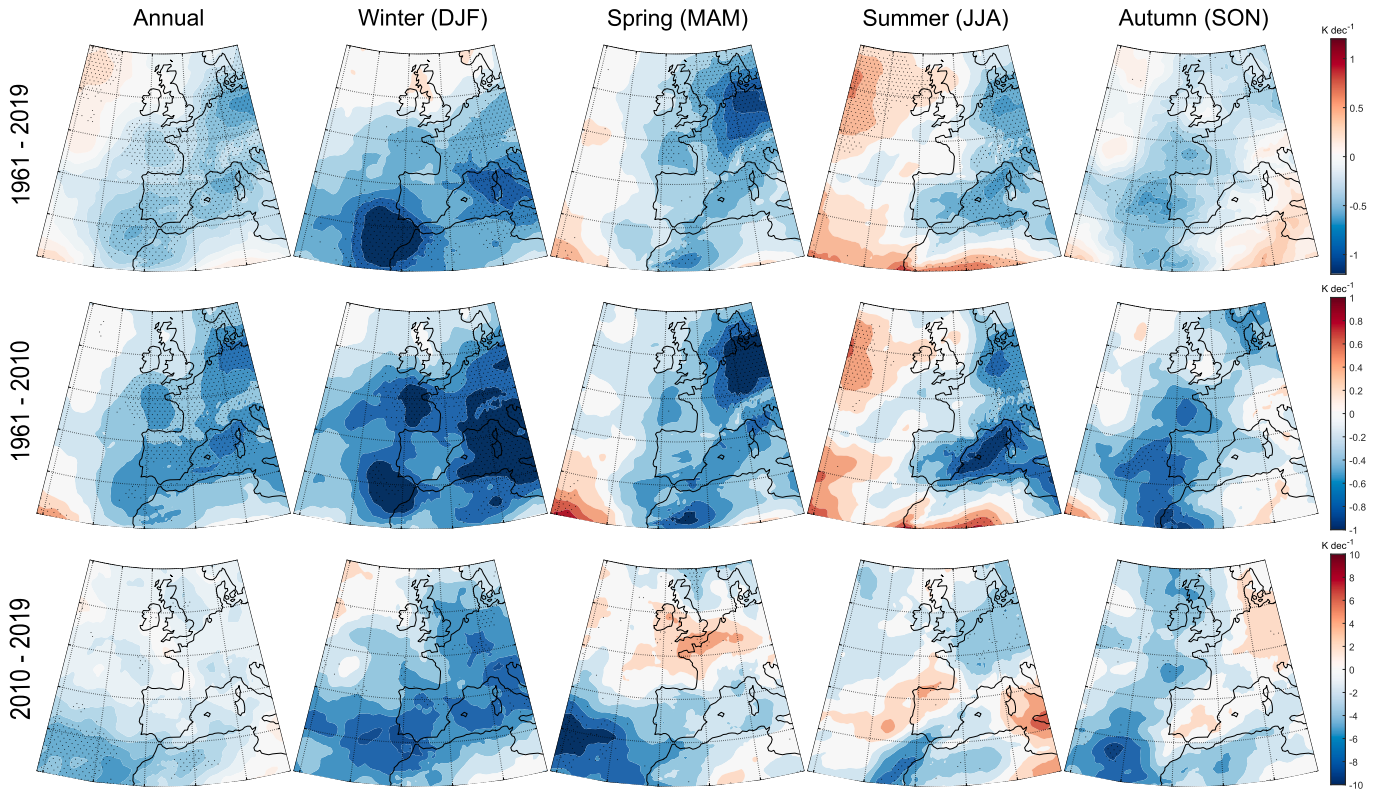

Fig. 11. Annual and seasonal trends (in $K dec^{-1}$) of the A index for 1961–2019, 1961–2010 and 2010–2019. Black dots indicate significant trends at $p < 0.05$. Different scales have been used for each period in order to appreciate trends.

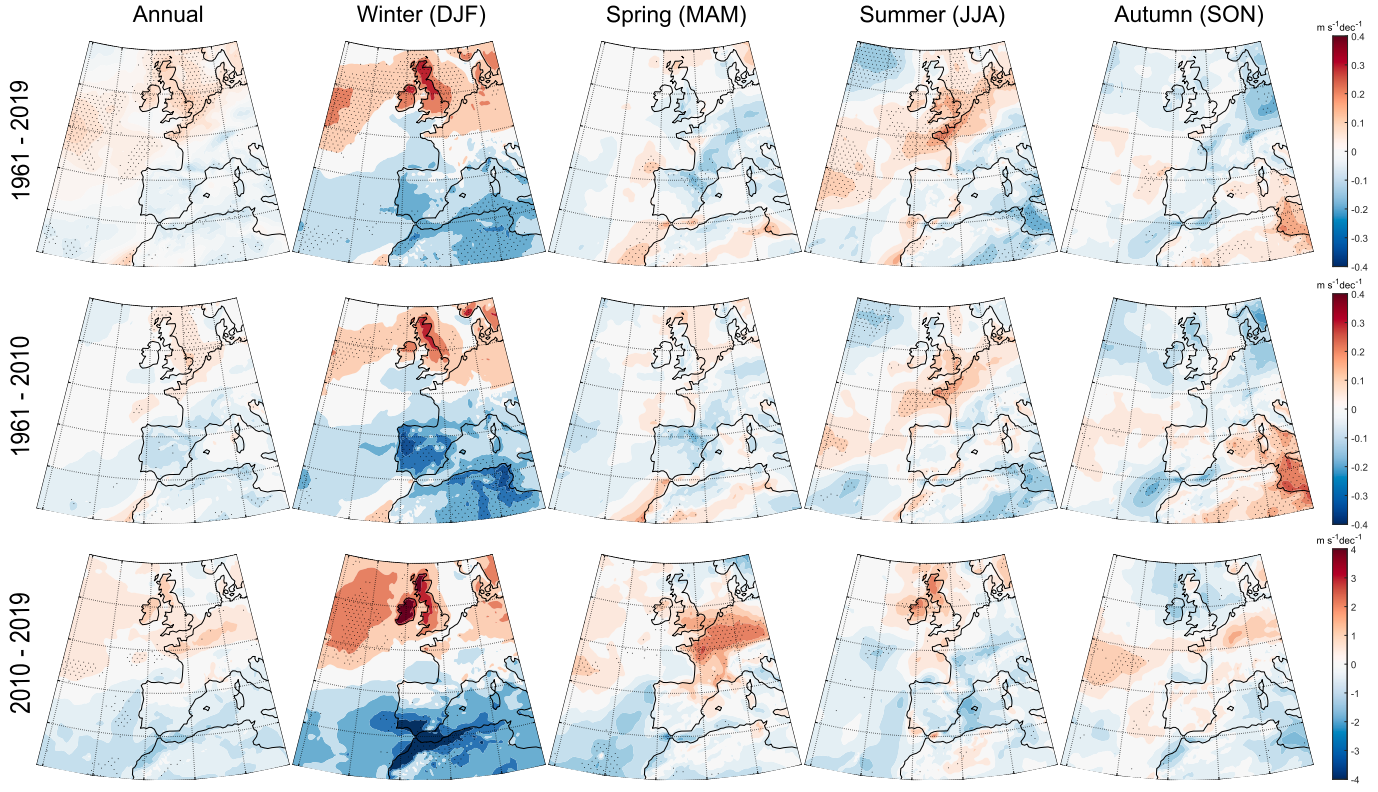

Fig. 12. Annual and seasonal trends (in $m s^{-1} dec^{-1}$) of the vertical wind shear (VWS) for 1961–2019, 1961–2010 and 2010–2019. Black dots indicate significant trends at $p < 0.05$. Different scales have been used for each period in order to appreciate trends.

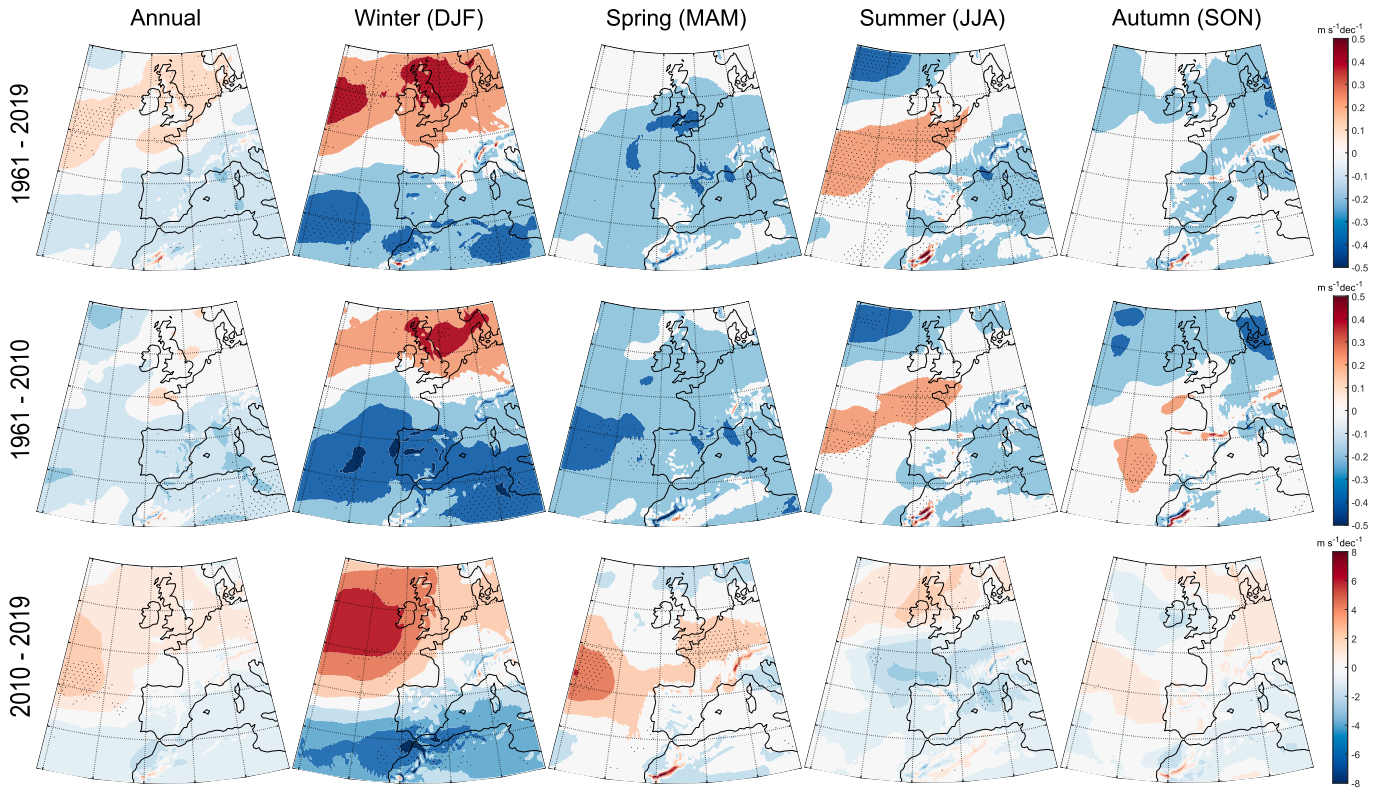

Fig. 13. Annual and seasonal trends (in $m s^{-1} dec^{-1}$) of the geostrophic wind for 1961–2019, 1961–2010 and 2010–2019. Black dots indicate significant trends at $p < 0.05$. Different scales have been used for each period in order to appreciate trends.

the industrial era limits our ability to assess the contributions of natural climate variability *versus* anthropogenic forcing on long-term changes in wind speed, both past and future. Therefore, it is highly desirable to extend the observational series beyond the 1960s to better attribute historical changes in wind speed on centennial scales. In recent times, 2021 was a year of exceptional low winds ("wind drough") in areas of UK and the North Atlantic Ocean. Therefore, the cessation of the *stilling* (or even *reversal*) could be a temporary event produced by the internal climate variability (Zeng et al., 2019) that has been superimposed on a negative trend of longer duration modulated by changes in the temperature gradient (Zhang et al., 2021) induced by anthropogenic greenhouse gas forcings (Deng et al., 2021, 2022). In fact, global surface winds are projected to continue weakening during the 21st century (Deng et al., 2021).

Even though the analysis included in this paper shed light over the *stilling* and *reversal* phenomena in the IP, and consequently contribute to generate a global picture, we should determine the influence of other climate drivers on the observed SWS and DPWG for a better understanding of its changes. The processes to be explored could be the surface roughness, the Atlantic Meridional Overturning Circulation (AMOC) or El Niño-Southern Oscillation (ENSO). There is still not enough knowledge about which have been the mechanisms that have triggered the *stilling* and *reversal* phenomena, how long the latter will last, what will be its magnitude or even if both phenomena will repeat as a cycle. This would have great impact in the energy industry since it would allow predicting the power generated by wind farms. Until climate models and reanalyses can accurately represent the near-surface wind speed and gusts (Minola et al., 2021a; Shen et al., 2021), analysis of observational data such as the one carried out here will be essential. They allow to determine the climatic evolution of winds and provide a basis on which to test the hypotheses of the physical mechanisms that are behind in a changing climate.

5. Conclusions

The principal findings of this research are:

- The occurrence of the cesation of the *stilling* phenomenon and a possible beginning of the *reversal* phenomenon in the last decades in the IP is confirmed for the first time. Its onset year varies considerably among seasons and across the three analysed wind parameters (namely, monthly mean near-surface wind speed, SWS; daily peak wind gust, DPWG; and number of days exceding the 90^{th} DPWG percentile), ranging from 1999 to 2018. It is worth mentioning that at the annual scale this onset occurs in 2007 approximately for the three variables studied; in summer, however, the *reversal* is not detected for any of them. Regarding its magnitude, the *reversal* period is still too short to gain statistically significant trends since the influence of inter-annual variability on the result is large.
- On annual scale, among the analysed teleconnection indices, WeMOi is the most correlated with the three wind parameters (significant positive correlation at $p < 0.05$). This finding remains for spring and autumn. In winter, NAOi and MOi present higher correlations than WeMOi, with a negative relationship. The *stilling* and *reversal* phenomena over the IP could be related to the trends observed in the WeMOi, since it has transitioned from decreasing during the 1961–2010 period to increasing in 2010–2019, especially in spring. In summer, this index shows a negative trend in both periods, which would be consistent with the continuation of the *stilling* phenomenon in this season.
- The correlations of the wind parameters with the frequency of occurrence of each Jenkinson and Collison weather type yield different results. In summer, the correlations are low in magnitude since mesoscale phenomena dominate. For the rest of the year, and especially in winter, relatively high positive and significant correlations appear with the W and NW types due to the influence of the jet stream, meanwhile relatively high negative and significant

correlations correspond to the A type since the Azores anticyclone causes calm days in the region. The *stilling* phenomenon in winter could be related to an increase in the frequency of the A type and a decrease in the W type.

- Both an increase in atmospheric thermal stability (from the A-index trends) and a northward shift of the jet stream (from the vertical wind shear and geostrophic wind trends) could be behind the possible causes of the *stilling* phenomenon. However, no clear explanations have been found for the *reversal* phenomenon by using the trends of the mentioned atmospheric parameters.

Data availability statement

Wind speed raw data from station observations were obtained from AEMET/IPMA. NAO index was retrieved from NOAA and from CRU, MO index was also retrieved from CRU, while WeMO index was downloaded from the Climate Group of the University of Barcelona. ERA5 Reanalysis were downloaded from ECMWF, and the JC scheme weather types classification is available upon request to the corresponding author.

CRediT authorship contribution statement

Eduardo Utrabo-Carazo: Conceptualization, Software, Formal analysis, Writing – original draft, Writing – review & editing. **Cesar Azorin-Molina:** Conceptualization, Methodology, Writing – review & editing, Supervision, Funding acquisition. **Encarna Serrano:** Conceptualization, Writing – review & editing. **Enric Aguilar:** Writing – review & editing. **Manola Brunet:** Writing – review & editing. **Jose A. Guijarro:** Data curation, Writing – review & editing.

Declaration of Competing Interest

None.

Acknowledgements

E.U.-C. was supported by the FPI fellowship (PRE2019-090148), and C.A.-M. by the Ramon y Cajal fellowship (RYC-2017-22830). This study was conducted in the framework of the IBER-STILLING project RTI2018-095749-A-100 (MCIU/AEI/FEDER,UE), the VENTS project AICO/2021/023 (GVA) and the CSIC Interdisciplinary Thematic Platform (PTI) *Clima*. (PTI-CLIMA). We acknowledge the anonymous reviewers for their detailed and helpful comments to the original manuscript.

Appendix A. Supplementary data

Supplementary data to this article can be found online at https://doi.org/10.1016/j.atmosres.2022.106153.

References

Alexandersson, H., 1986. A homogeneity test applied to precipitation data. Int. J. Climatol. 12, 661–675. https://doi.org/10.1002/joc.3370060607.

Allen, R.J., Kovilakam, M., 2017. The role of natural climate variability in recent tropical expansion. J. Clim. 30, 6329–6350. https://doi.org/10.1175/JCLI-D-16-0735.1.

Azorin-Molina, C., Cheng, D., Tijm, S., Baldi, M., 2011. A multi-year study of sea breezes in a Mediterranean coastal site: Alicante (Spain). Int. J. Climatol. 31, 468–486. https://doi.org/10.1002/joc.2064.

Azorin-Molina, C., Vicente-Serrano, S.M., Mcvicar, T.R., Jerez, S., Sanchez-Lorenzo, A., López-Moreno, J.I., Revuelto, J., Trigo, R.M., Lopez-Bustins, J.A., Espírito-Santo, F., 2014. Homogenization and assessment of observed near-surface wind speed trends over Spain and Portugal, 1961–2011. J. Clim. 27, 3692–3712. https://doi.org/10.1175/JCLI-D-13-00652.1.

Azorin-Molina, C., Guijarro, J.A., Mcvicar, T.R., Vicente-Serrano, S.M., Chen, D., Jerez, S., Espirito-Santo, F., 2016. Trends of daily peak wind gusts in Spain and Portugal, 1961–2014. J. Geophys. Res. Atmos. 121, 1059–1078. https://doi.org/10.1002/2015JD024485.

Azorin-Molina, C., Asin, J., McVicar, T.R., Minola, L., Lopez-Moreno, J.I., Vicente-Serrano, S.M., Chen, D., 2018a. Evaluating anemometer drift: a statistical approach to correct biases in wind speed measurement. Atmos. Res. 203, 175–188. https://doi.org/10.1016/j.atmosres.2017.12.010.

Azorin-Molina, C., Rehman, S., Guijarro, J.A., McVicar, T.R., Minola, L., Chen, D., Vicente-Serrano, S.M., 2018b. Recent trends in wind speed across Saudi Arabia, 1978–2013: a break in the stilling. Int. J. Climatol. 38, 966–984. https://doi.org/10.1002/joc.5423.

Azorin-Molina, C., McVicar, T.R., Guijarro, J.A., Trewin, B., Frost, A.J., Zhang, G., Minola, L., Son, S.-W., Deng, K., Chen, D., 2021. A decline of observed daily peak wind gusts with distinct seasonality in Australia, 1941–2016. J. Clim. 34, 3103–3127. https://doi.org/10.1175/JCLI-D-20-0590.1.

Barnes, E.A., Polvani, L., 2013. Response of the midlatitude jets, and of their variability, to increased greenhouse gases in the CMIP5 models. J. Clim. 26, 7117–7135. https://doi.org/10.1175/JCLI-D-12-00536.1.

Barnston, A.G., Livezey, R.E., 1987. Classification, seasonality and persistence of low-frequency atmospheric circulation patterns. Mon. Wea. Rev. 115, 1083–1126. https://doi.org/10.1175/1520-0493(1987)115<1083:CSAPOL>2.0.CO;2.

Bell, B., Hersbach, H., Berrisford, P., Dahlgren, P., Horányi, A., Muñoz Sabater, J., Nicolas, J., Radu, R., Schepers, D., Simmons, A., Soci, C., Thépaut, J.-N., 2020a. ERA5 Monthly Averaged Data on Pressure Levels From 1950 to 1978 (Preliminary Version). Accessed 16 December 2021. https://cds.climate.copernicus.eu/.

Bell, B., Hersbach, H., Berrisford, P., Dahlgren, P., Horányi, A., Muñoz Sabater, J., Nicolas, J., Radu, R., Schepers, D., Simmons, A., Soci, C., Thépaut, J.-N., 2020b. ERA5 Monthly Averaged Data on Single Levels From 1950 to 1978 (Preliminary Version). Accessed 16 December 2021. https://cds.climate.copernicus.eu/.

Brázdil, R., Hostýnek, J., Řezníčková, L., Zahradníček, P., Tolasz, R., Dobrovolný, P., Štěpánek, P., 2017. The variability of maximum wind gusts in the Czech Republic between 1961 and 2014. Int. J. Climatol. 37, 1961–1978. https://doi.org/10.1002/joc.4827.

Brunetti, M., Caloiero, T., Coscarelli, R., Gullà, G., Nanni, T., Simolo, C., 2010. Precipitation variability and change in the Calabria region (Italy) from a high resolution daily dataset. Int. J. Climatol. 32, 57–73. https://doi.org/10.1002/joc.2233.

Criado-Aldeabuena, F., Soto-Navarro, F.J., 2013. The mediterranean oscillation teleconnection index: station-based versus principal component paradigms. Adv. Meteorol. 2013, 738501 https://doi.org/10.1155/2013/738501.

Davis, N., Birner, T., 2017. On the discrepancies in tropical belt expansion between reanalyses and climate models and among tropical belt width metrics. J. Clim. 30, 1211–1231. https://doi.org/10.1175/JCLI-D-16-0371.1.

Deng, K., Azorin-Molina, C., Minola, L., Zhang, G., Chen, D., 2021. Global near-surface wind speed changes over the last decades revealed by reanalyses and CMIP6 model simulations. J. Clim. 34, 2219–2234. https://doi.org/10.1175/JCLI-D-20-0310.1.

Deng, K., Azorin-Molina, C., Yang, S., Hu, C., Zhang, G., Minola, L., Chen, D., 2022. Changes of southern hemisphere westerlies in the future warming climate. Atmos. Res. 270, 106040 https://doi.org/10.1016/j.atmosres.2022.106040.

Deser, C., 2020. Certain uncertainty: the role of internal climate variability in projections of regional climate change and risk management. Earth's Future 8. https://doi.org/10.1029/2020EF001854 e2020EF001854.

Finné, M., Woodbridge, J., Labuhn, I., Roberts, C.N., 2019. Holocene hydro-climatic variability in the mediterranean: a synthetic multi-proxy reconstruction. Holocene 29, 847–863. https://doi.org/10.1177/0959683619826634.

García-Valero, J.A., Montavez, J.P., Jerez, S., Gómez-Navarro, J.J., Lorente-Plazas, R., Jiménez-Guerrero, P., 2012. A seasonal study of the atmospheric dynamics over the Iberian Peninsula based on circulation types. Theor. Appl. Climatol. 110, 291–310. https://doi.org/10.1007/s00704-012-0623-0.

Ge, J., Feng, D., You, Q., Zhang, W., Zhang, Y., 2021. Characteristics and causes of surface wind speed variations in Northwest China from 1979 to 2019. Atmos. Res. 254, 105527 https://doi.org/10.1016/j.atmosres.2021.105527.

Grise, K.M., Davis, S.M., Simpson, I.R., Waugh, D.W., Fu, Q., Allen, R.J., Rosenlof, K.H., Ummenhofer, C.C., Karnauskas, K.B., Maycock, A.C., Quan, X.W., Birner, T., Staten, P.W., 2019. Recent tropical expansion: natural variability or forced response? J. Clim. 32, 1551–1571. https://doi.org/10.1175/JCLI-D-18-0444.1.

Guo, H., Xu, M., Hu, Q., 2011. Changes in near-surface wind speed in China: 1969-2005. Int. J. Climatol. 31, 349–358. https://doi.org/10.1002/joc.2091.

Hamed, K.H., Rao, A.R., 1998. A modified Mann-Kendall trend test for autocorrelated data. J. Hydrol. 204, 182–196. https://doi.org/10.1016/S0022-1694(97)00125-X.

He, Y., Wu, B., He, P., Gu, W., Liu, B., 2021. Wind disasters adaptation in cities in a changing climate: a systematic review. PLoS One 16, e0248503. https://doi.org/10.1371/journal.pone.0248503.

Hersbach, H., Bell, B., Berrisford, P., Biavati, G., Horányi, A., Muñoz Sabater, J., Nicolas, J., Peubey, C., Radu, R., Rozum, I., Schepers, D., Simmons, A., Soci, C., Dee, D., Thépaut, J.-N., 2019a. ERA5 Monthly Averaged Data on Pressure Levels From 1979 to Present. Accessed 16 December 2021. https://doi.org/10.24381/cds.6860a573.

Hersbach, H., Bell, B., Berrisford, P., Biavati, G., Horányi, A., Muñoz Sabater, J., Nicolas, J., Peubey, C., Radu, R., Rozum, I., Schepers, D., Simmons, A., Soci, C., Dee, D., Thépaut, J.-N., 2019b. ERA5 Monthly Averaged Data on Single Levels From 1979 to Present. Accessed 16 December 2021. https://doi.org/10.24381/cds.f17050d7.

Hou, A., Ni, G., Yang, H., Lei, Z., 2013. Numerical analysis on the contribution of urbanization to wind stilling: an example over the greater Beijing metropolitan area. J. Appl. Meteorol. Climatol. 52, 1105–1115. https://doi.org/10.1175/JAMC-D-12-013.1.

IPCC, 2013. Climate Change 2013: The Physical Science Basis. Cambridge University Press. https://doi.org/10.1017/CBO9781107415324.

Jenkinson, A.F., Collison, B.P., 1977. An Initial Climatology of Gales Over the North Sea. Synoptic Climatol. Branch Memo. 62 Met Office Bracknell, U. K.

Jiménez, P.A., González-Rouco, F., Montávez, J.P., García-Bustamante, E., Navarro, J., 2008. Climatology of wind patterns in the northeast of the Iberian Peninsula. Int. J. Climatol. 29, 501–525. https://doi.org/10.1002/joc.1705.
Jones, P.D., Jonsson, T., D., W., 1997. Extension to the North Atlantic Oscillation using early instrumental pressure observations from Gibraltar and South-West Iceland. Int. J. Climatol. 17, 1433–1450. https://doi.org/10.1002/(SICI)1097-0088(19971115)17:13<1433::AID-JOC203>3.0.CO;2-P.
Kahru, M., Gille, S.T., Murtugudde, R., Strutton, P.G., Manzano-Sarabia, M., Wang, H., Mitchell, B.G., 2010. Global correlations between winds and ocean chlorophyll. J. Geophys. Res. 115, C12040. https://doi.org/10.1029/2010JC006500.
Kendall, M.G., Gibbons, J.D., 1990. Rank Correlation Methods. Oxford University Press.
Kim, J., Paik, K., 2015. Recent recovery of surface wind speed after decadal decrease: a focus on South Korea. Clim. Dyn. 45, 1699–1712. https://doi.org/10.1007/s00382-015-2546-9.
Li, Y., Chen, Y., Li, Z., Fang, G., 2018. Recent recovery of surface wind speed in Northwest China. Int. J. Climatol. 38, 4445–4458. https://doi.org/10.1002/joc.5679.
Li, Y., Chen, Y., Li, Z., 2019. Effects of land use and cover change on surface wind speed in China. J. Arid Land 11, 345–356. https://doi.org/10.1007/s40333-019-0095-5.
Lorente-Plazas, R., Montávez, J.P., Jimenez, P.A., Jerez, S., Gómez-Navarro, J.J., García-Valero, J.A., Jimenez-Guerrero, P., 2015. Characterization of surface winds over the Iberian Peninsula. Int. J. Climatol. 35, 1007–1026. https://doi.org/10.1002/joc.4034.
Mantsis, D.F., Sherwood, S., Allen, R., Shi, L., 2017. Natural variations of tropical width and recent trends. Geophys. Res. Lett. 44, 3825–3832. https://doi.org/10.1002/2016GL072097.
Martin-Vide, J., Lopez-Bustins, J.-A., 2006. The Western Mediterranean Oscillation and rainfall in the Iberian Peninsula. Int. J. Climatol. 26, 1455–1475. https://doi.org/10.1002/joc.1388.
McVicar, T.R., Van Niel, T.G., Li, L.T., Roderick, M.L., Rayner, D.P., Ricciardulli, L., Donohue, R.J., 2008. Wind speed climatology and trends for Australia, 1975–2006: capturing the stilling phenomenon and comparison with near-surface reanalysis output. Geophys. Res. Lett. 35, L20403. https://doi.org/10.1029/2008GL035627.
McVicar, T.R., Van Niel, T.G., Roderick, M.L., Li, L.T., Mo, X.G., Zimmermann, N.E., Schmatz, D.R., 2010. Observational evidence from two mountainous regions that near-surface wind speeds are declining more rapidly at higher elevations than lower elevations: 1960–2006. Geophys. Res. Lett. 37, L06402 https://doi.org/10.1029/2009GL042255.
McVicar, T.R., Roderick, M.L., Donohue, R.J., Li, L.T., Van Niel, T.G., Thomas, A., Grieser, J., Jhajharia, D., Himri, Y., Mahowald, N.M., Mescherskaya, A.V., Kruger, A. C., Rehman, S., Dinpashoh, Y., 2012a. Global review and synthesis of trends in observed terrestrial near-surface wind speeds: implications for evaporation. J. Hydrol. 416–417, 182–205. https://doi.org/10.1016/j.jhydrol.2011.10.024.
McVicar, T.R., Roderick, M.L., Donohue, R.J., Van Niel, T.G., 2012b. Less bluster ahead? Ecohydrological implications of global trends of terrestrial near-surface wind speeds. Ecohydrology 5, 381–388. https://doi.org/10.1002/eco.1298.
Minola, L., Azorin-Molina, C., Chen, D., 2016. Homogenization and assessment of observed near-surface wind speed trends across Sweden, 1956-2013. J. Clim. 29, 7397–7415. https://doi.org/10.1175/JCLI-D-15-0636.1.
Minola, L., Azorin-Molina, C., Guijarro, J.A., Zhang, G., Son, S.-W., Chen, D., 2021a. Climatology of near-surface daily peak wind gusts across Scandinavia: observations and model simulations. J. Geophys. Res. Atmos. 126 https://doi.org/10.1029/2020JD033534 e2020JD033534.
Minola, L., Reese, H., Lai, H.-W., Azorin-Molina, C., Guijarro, J.A., Son, S.-W., Chen, D., 2021b. Wind stilling-reversal across sweden: the impact of land-use and large-scale atmospheric circulation changes. Int. J. Climatol. https://doi.org/10.1002/joc.7289 n/a, n/a.
Molina, M.O., Gutiérrez, C., Sánchez, E., 2021. Comparison of ERA5 surface wind speed climatologies over Europe with observations from the HadISD dataset. Int. J. Climatol. 41, 4864–4878. https://doi.org/10.1002/joc.7103.
Muggeo, V.M.R., 2003. Estimating regression models with unknown break-points. Stat. Med. 22, 3055–3071. https://doi.org/10.1002/sim.1545.
Muggeo, V.M.R., 2016. Testing with a nuisance parameter present only under the alternative: a score-based approach with application to segmented modelling. J. Stat. Comput. Simul. 86, 3059–3067. https://doi.org/10.1080/00949655.2016.1149855.
Nicholls, N., 2001. The insignificance of significance testing. Bull. Am. Meteor. Soc. 82, 981–986. https://doi.org/10.2307/3802789.
Obermann-Hellhund, A., Conte, D., Somot, S., Torma, C.Z., Ahrens, B., 2018. Mistral and Tramontane wind systems in climate simulations from 1950 to 2100. Clim. Dyn. 50, 693–703. https://doi.org/10.1007/s00382-017-3635-8.
Otero, N., Sillmann, J., Butler, T., 2018. Assessment of an extended version of the Jenkinson–Collison classification on CMIP5 models over Europe. Clim. Dyn. 50, 1559–1579. https://doi.org/10.1007/s00382-017-3705-y.
Palutikov, J., 2003. Analysis of mediterranean climate data: measured and modelled. In: Bolle, H.-J. (Ed.), *Mediterranean Climate: Variability and Trends.* Regional Climate Studies. Springer, pp. 125–132.
Pinto, J.G., Raible, C.C., 2012. Past and recent changes in the North Atlantic oscillation. WIREs Clim. Change 3, 79–90. https://doi.org/10.1002/wcc.150.
Pisano, A., Marullo, S., Artale, V., Falcini, F., Yang, C., Leonelli, F.E., Santoleri, R., Buongiorno Nardelli, B., 2020. New evidence of mediterranean climate change and variability from sea surface temperature observations. Remote Sens. 12, 132. https://doi.org/10.3390/rs12010132.
Pryor, S.C., Barthelmie, R.J., Young, D.T., Takle, E.S., Arritt, R.W., Flory, D., Gutowski, W.J., Nunes, A., Roads, J., 2009. Wind speed trends over the contiguous United States. J. Geophys. Res. Atmos. 114, D14105 https://doi.org/10.1029/2008JD011416.
Ramon, J., Lledó, L., Torralba, V., Soret, A., Doblas-Reyes, F.J., 2019. What global reanalysis best represents near-surface winds? Q. J. R. Meteorol. Soc. 145, 3236–3251. https://doi.org/10.1002/qj.3616.
Roderick, M.L., Rotstayn, L.D., Farquhar, G.D., Hobbins, M.T., 2007. On the attribution of changing pan evaporation. Geophys. Res. Lett. 34, L17403. https://doi.org/10.1029/2007GL031166.
Rousi, E., Rust, H.W., Ulbrich, U., Anagnostopoulou, C., 2020. Implications of winter NAO flavors on present and future European climate. Climate 8, 13. https://doi.org/10.3390/cli8010013.
Shen, C., Zha, J., Wu, J., Zhao, D., Azorin-Molina, C., Fan, W., Yu, Y., 2021. Does cra-40 outperform other reanalysis products in evaluating near-surface wind speed changes over China? Atmos. Res. 266, 105948 https://doi.org/10.1016/j.atmosres.2021.105948.
Shepherd, T.G., 2014. Atmospheric circulation as a source of uncertainty in climate change projections. Nat. Geosci. 7, 703–708. https://doi.org/10.1038/ngeo2253.
Stull, R.B., 1988. An Introduction to Boundary Layer Meteorology. Springer.
Sun, C., Liu, L., Li, L.-J., Wang, B., Zhang, C., Liu, Q., Li, R.-Z., 2018. Uncertainties in simulated el niño–southern oscillation arising from internal climate variability. Atmos. Sci. Lett. 19, e805 https://doi.org/10.1002/asl.805.
Tian, Q., Huang, G., Hu, K., Niyogi, D., 2019. Observed and global climate model based changes in wind power potential over the Northern Hemisphere during 1979–2016. Energy 167, 1224–1235. https://doi.org/10.1016/j.energy.2018.11.027.
Torralba, V., Doblas-Reyes, F.J., Gonzalez-Reviriego, N., 2017. Uncertainty in recent near-surface wind speed trends: a global reanalysis intercomparison. Environ. Res. Lett. 12, 114019 https://doi.org/10.1088/1748-9326/aa8a58.
Vautard, R., Cattiaux, J., Yiou, P., Thépaut, J.-N., Ciais, P., 2010. Northern Hemisphere atmospheric stilling partly attributed to an increase in surface roughness. Nat. Geosci. 3, 756–761. https://doi.org/10.1038/ngeo979.
Vicente-Serrano, S.M., Trigo, R.M., 2011. Hydrological, Socioeconomic and Ecological Impacts of the North Atlantic Oscillation in the Mediterranean Region. Springer.
Wan, H., Wang, X.L., Swail, V.R., 2010. Homogenization and trend analysis of Canadian near-surface wind speeds. J. Clim. 23, 1209–1225. https://doi.org/10.1175/2009JCLI3200.1.
Watt-Meyer, O., Frierson, D.M., Fu, Q., 2019. Hemispheric asymmetry of tropical expansion under CO2 forcing. Geophys. Res. Lett. 46, 9231–9240. https://doi.org/10.1029/2019GL083695.
Weatherhead, E.C., Reinsel, G.C., Tiao, G.C., Meng, X.-L., Choi, D., Cheang, W.-K., Keller, T., DeLuisi, J., Wuebbles, D.J., Kerr, J.B., Miller, A.J., Oltmans, S.J., Frederick, J.E., 1998. Factors affecting the detection of trends: statistical considerations and applications to environmental data. J. Geophys. Res. 103, 17149–17161. https://doi.org/10.1029/98JD00995.
Wever, N., 2012. Quantifying trends in surface roughness and the effect on surface wind speed observations. J. Geophys. Res. Atmos. 117, D11104 https://doi.org/10.1029/2011JD017118.
WMO, 1987. In: Beljaars, A.C.M. (Ed.), The Measurement of Gustiness at Routine Wind Stations: A Review, Instruments and Observing Methods Report No. 31. Geneva.
Wohland, J., Omrani, N.-E., Witthaut, D., Keenlyside, N.S., 2019. Inconsistent wind speed trends in current twentieth century reanalyses. J. Geophys. Res. Atmos. 124, 1931–1940. https://doi.org/10.1029/2018JD030083.
Wohland, J., Folini, D., Pickering, B., 2021. Wind speed stilling and its recovery due to internal climate variability. Earth Syst. Dynam. 12, 1239–1251. https://doi.org/10.5194/esd-2021-29.
Wu, J., Zha, J., Zhao, D., Yang, Q., 2018. Changes in terrestrial near-surface wind speed and their possible causes: an overview. Clim. Dyn. 51, 2039–2078. https://doi.org/10.1007/s00382-017-3997-y.
Young, I.R., Ribal, A., 2019. Multiplatform evaluation of global trends in wind speed and wave height. Science 364, 548–552. https://doi.org/10.1126/science.aav9527.
Zeng, Z., Piao, S., Li, L.Z.X., Ciais, P., Li, Y., Cai, X., Yang, L., Liu, M., Wood, E.F., 2018. Global terrestrial stilling: does Earth's greening play a role? Environ. Res. Lett. 13, 124013 https://doi.org/10.1088/1748-9326/aaea84.
Zeng, Z., Ziegler, A.D., Searchinger, T., Yang, L., Chen, A., Ju, K., Piao, S., Li, L.Z.X., Ciais, P., Chen, D., Liu, J., Azorin-Molina, C., Chappell, A., Medvigy, D., Wood, E.F., 2019. A reversal in global terrestrial stilling and its implications for wind energy production. Nat. Clim. Chang. 9, 979–985. https://doi.org/10.1038/s41558-019-0622-6.
Zha, J., Zhao, D., Tang, J., 2019. A possible recovery of the near-surface wind speed in Eastern China during winter after 2000 and the potential causes. Theor. Appl. Climatol. 136, 119–134. https://doi.org/10.1007/s00704-018-2471-z.
Zhang, Z., Wang, K., 2020. Stilling and recovery of the surface wind speed based on observation, reanalysis, and geostrophic wind theory over China from 1960 to 2017. J. Clim. 33, 3989–4008. https://doi.org/10.1175/JCLI-D-19-0281.1.
Zhang, R., Li, Q., Zhang, R., 2013. Meteorological conditions for the persistent severe fog and haze event over eastern China in January 2013. Sci. China Earth Sci. 57, 26–35. https://doi.org/10.1007/s11430-013-4774-3.
Zhang, Z., Wang, K., Chen, D., Li, J., Dickinson, R., 2019. Increase in surface friction dominates the observed surface wind speed decline during 1973–2014 in the northern hemisphere lands. J. Clim. 32, 7421–7435. https://doi.org/10.1175/JCLI-D-18-0691.1.
Zhang, G., Azorin-Molina, C., Chen, D., Guijarro, J.A., Kong, F., Minola, L., McVicar, T. R., Son, S.-W., Shi, P., 2020. Variability of daily maximum wind speed across China,

1975–2016 : an examination of likely causes. J. Clim. 33, 2793–2816. https://doi.org/10.1175/JCLI-D-19-0603.1.

Zhang, G., Azorin-Molina, C., Chen, D., McVicar, T.R., Guijarro, J.A., Kong, F., Minola, L., Deng, K., Shi, P., 2021. Uneven warming likely contributed to declining near-surface wind speeds in northern China between 1961 and 2016. J. Geophys. Res. Atmos. 126 https://doi.org/10.1029/2020JD033637 e2020JD033637.

Zurita-Gotor, P., Álvarez Zapatero, P., 2018. Coupled interannual variability of the Hadley and Ferrel cells. J. Clim. 31, 4757–4773. https://doi.org/10.1175/JCLI-D-17-0752.1.